

The University of Maine

DigitalCommons@UMaine

Electronic Theses and Dissertations

Fogler Library

Summer 8-18-2023

Exploring the Use of Audible Sound in Bone Density Diagnostic Devices

Evan J. Bess
evan.bess@maine.edu

Follow this and additional works at: <https://digitalcommons.library.umaine.edu/etd>



Part of the [Biomedical Commons](#), [Biomedical Devices and Instrumentation Commons](#), and the [Signal Processing Commons](#)

Recommended Citation

Bess, Evan J., "Exploring the Use of Audible Sound in Bone Density Diagnostic Devices" (2023). *Electronic Theses and Dissertations*. 3819.

<https://digitalcommons.library.umaine.edu/etd/3819>

This Open-Access Thesis is brought to you for free and open access by DigitalCommons@UMaine. It has been accepted for inclusion in Electronic Theses and Dissertations by an authorized administrator of DigitalCommons@UMaine. For more information, please contact um.library.technical.services@maine.edu.

**EXPLORING THE USE OF AUDIBLE SOUND IN BONE DENSITY
DIAGNOSTIC DEVICES**

By

Evan Bess

B.S. University of Maine, 2022

A THESIS

Submitted in Partial Fulfillment of the
Requirements for the Degree of
Master of Science
(in Biomedical Engineering)

The Graduate School

The University of Maine

August 2023

Advisory Committee:

Michael Mason, Professor of Chemical and Biomedical Engineering, Advisor

Todd O'Brien, Adjunct Professor of Chemical and Biomedical Engineering

Bruce Segee, Professor of Electrical and Computer Engineering

Copyright 2023 Evan Bess

All Rights Reserved

**EXPLORING THE USE OF AUDIBLE SOUND IN BONE DENSITY
DIAGNOSTIC DEVICES**

By Evan Bess

Thesis Advisor: Dr. Michael Mason

An Abstract of the Thesis Presented
in Partial Fulfillment of the Requirements for the
Degree of Master of Science
(in Biomedical Engineering)
August 2023

Osteoporosis is a medical condition in which there is a progressive degradation of bone tissue that correlates with a characteristic decrease in bone density (BD). It is estimated that osteoporosis affects over 200 million people globally and is responsible for 8.9 million fractures annually. Populations at risk for developing osteoporosis include post-menopausal women, diabetic patients, and the elderly, representing a large population within the state of Maine. Current densitometric and sonometric devices used to monitor BD include quantitative computed tomography (QCT), dual-energy x-ray absorption (DXA), and ultrasound (QUS). All methods are expensive and, in the cases of QCT and DXA, patients are exposed to small, frequent doses of ionizing radiation. While these methods can effectively measure BD, they are critically limited for applications in rural healthcare because they are cost-prohibitive to rural medical facilities and to patients that require routine screening. The diversity of at-risk patient populations, current expensive and invasive BD devices drives the need for a rapid, low-cost, and non-invasive approach to monitoring BD. The present work explores audible sound as a potential solution that could safely and effectively measure BD by minimizing cost drivers and increasing device

simplicity to improve availability. The current prototype aims to measure calcaneal (heel) BD using audible sound and time delay spectroscopy (TDS).

To assess the feasibility of such a device, iterative prototypes were constructed and evaluated, a relative sensitivity analysis was performed, and testing of critical device components was completed. The testing included the ability of the device to measure the frequency and phase of a signal, measure the coupling force applied at the patient and device interface, and measure the geometries of a test material. The relative sensitivity analysis supported the use of audible sound in this application. The testing showed the device can measure the frequency and phase of a signal and the geometries of a test material while design changes are required to measure the coupling force. With the indicated improvements, the device is ready for testing materials that share similar material properties with bone.

ACKNOWLEDGEMENTS

I would like to thank my advisor, Professor Michael Mason, for allowing me to conduct research in his lab. I appreciate all the knowledge, advice, and support he has shared during my time at the University of Maine. I would like to thank Dr. Todd O'Brien for providing his clinical expertise and foundational work on the project. I would like to thank Professor Bruce Segee for sharing his knowledge of electrical and computer engineering. I would like to thank Forrest Flagg, Renee Kelley, Professor Robert Bowie, and Professor Karissa Tilbury for their advice and support on this project. I am grateful to everyone in the Mason Lab research group who helped me during my graduate studies. This includes William Cassidy who worked as an undergraduate student on the project. I would like to acknowledge all my friends who have supported me during my time at the University of Maine. Last, but certainly not least, I would like to thank my family for their love and support.

TABLE OF CONTENTS

ACKNOWLEDGEMENTS	iii
LIST OF TABLES	viii
LIST OF FIGURES	ix
LIST OF EQUATIONS	xiv
1. INTRODUCTION	1
1.1. Background	1
1.2. Thesis Objectives	2
1.3. Thesis Layout	2
2. LITERATURE REVIEW	3
2.1. Introduction	3
2.2. Bone Diagnostic Specialties	3
2.2.1. Osteoporosis	4
2.2.2. Bone Densitometry	7
2.2.3. Bone Sonometry	11
2.2.4. Bone Densitometric/Sonometric System	14
2.2.5. Recommendations for Bone Health Assessments in Rural and Global Health Applications	16
2.3. Physics of Sound	17
2.4. Bone Structure	19

2.5. Time Delay Spectroscopy (TDS).....	20
2.6. Prospective Markets.....	21
2.7. Four-Woodlock Sales Forecast.....	23
2.8. Food and Drug Administration (FDA) Approval Process for Medical Devices	24
2.8.1. Proposed Device Classification	26
2.9. Summary	28
3. DEVICE DEVELOPMENT	29
3.1. Methods.....	29
3.1.1. Computational Method	29
3.1.2. Deliverables	31
3.2. Device Sensitivity	32
3.2.1. Relative Sensitivity Analysis	32
3.2.2. Microphone Position Sensitivity.....	34
3.3. Device Hardware	37
3.3.1. Alpha (α) Prototype	37
3.3.2. Test Bed - Beta (β) Prototype	39
3.3.3. Cost.....	42
3.4. LabVIEW Virtual Instruments (VI).....	44
3.5. Device Resolution.....	46
3.6. Device Safety	47

4. EXPERIMENTS	49
4.1. Frequency and Phase Experiment	49
4.1.1. Introduction.....	49
4.1.2. Methods.....	49
4.1.3. Results.....	52
4.1.4. Discussion.....	55
4.1.5. Conclusions.....	58
4.2. Actuator Coupling Force & Speed.....	58
4.2.1. Introduction.....	58
4.2.2. Methods.....	59
4.2.3. Results.....	61
4.2.4. Discussion.....	64
4.2.5. Conclusions.....	67
4.3. Software Timed Distance Measurement.....	67
4.3.1. Introduction.....	67
4.3.2. Methods.....	68
4.3.3. Results.....	69
4.3.4. Discussion.....	70
4.3.5. Conclusion	72
4.4. Summary of Experimental Results	72

5. RECOMMENDATIONS FOR THE FUTURE.....	73
REFERENCES	76
APPENDIX: ADDITIONAL INFORMATION ON SONOMETRIC & DENSITOMETRIC TECHNIQUES	82
BIOGRAPHY OF THE AUTHOR.....	84

LIST OF TABLES

Table 2.1.	US Nuclear Regulatory Commission (NRC) occupational dose limits. Reproduced from ref (37).....	11
Table 2.2.	FDA classification of medical devices. Reproduced from ref (61).....	26
Table 2.3.	FDA-predicated or equivalent for bone sonometers reproduced from The US Food and Drug Administration. Reproduced from ref (59).....	27
Table 3.1.	Normal operating points of the variables used in the governing equation. All values are based on that of trabecular bone and ultrasound wave propagation.....	33
Table 3.2.	Hardware materials list for the alpha (α) and beta (β) prototype.....	43
Table 4.1.	Specifications for a 4” PA-07 Series Micro Linear Actuator from Progressive Automations.....	60
Table 4.2.	The intercept, slope, standard error (SE), and the adjusted R-square value for the load versus current calibration data.....	61
Table 4.3.	The intercept, slope, standard error (SE), and the adjusted R-square value for the load versus speed calibration data.....	63
Table 4.4.	Shows the load applied to the actuator, the speed used to predict the expected distance, the average standard error between the expected distance and measured distance, and the RRMSE of the expected distance and measured distance.....	70
Table A.1.	Additional information on sonometric and densitometric techniques.....	82

LIST OF FIGURES

Figure 2.1.	SEM image of normal (A) and osteoporotic bone (B). Reproduced from ref (17).....	4
Figure 2.2.	Representation of BD over time in male and female populations.....	6
Figure 2.3.	Report of a DXA scan of the hips and spine (left) scanner and the GE Healthcare Lunar iDXA scanner (right). Adapted from ref (24).....	9
Figure 2.4.	Anterior 2D QCT scan of the human spine reproduced from ref (30) (left) and GE GoldSeal Optima CT660 QCT scanner (right) adapted from GE Health ref (31) (right).....	9
Figure 2.5.	Report (left) generated from a heel assessment using the GE Lunar Achilles ultrasound device (right). Adapted from ref (39).....	12
Figure 2.6.	System map of the densitometric and sonometric system.....	14
Figure 2.7.	A heat map that was generated to evaluate the current methods of assessing bone health from a rural and global health initiative prospective.....	16
Figure 2.8.	A simplified diagram showing that the velocity of sound is the fastest in dense solids and slower in less dense solids.....	17
Figure 2.9.	Sound spectrum identifying the frequency ranges of infrasound, audible sound, and ultrasound.....	18
Figure 2.10.	Shows the bone hierarchy from the macrostructure to the sub-nanostructure. Adapted from ref (15).....	19

Figure 2.11.	Application of TDS on two arbitrary signals 1 and 2 of the same frequency.....	20
Figure 2.12.	A graph plotting the minimum and maximum recorded speeds of ultrasound (used to estimate the behavior of audible sound) across the minimum and maximum North American heel thickness.....	21
Figure 3.1.	Cartoon of the device and physical geometry.....	29
Figure 3.2.	Example of the electrical signals used in TDS.....	31
Figure 3.3.	Graph of the log scale propagation time sensitivity across the range of expected heel thickness.....	34
Figure 3.4.	Microphone positioning scenarios used for the microphone positioning sensitivity analysis.....	35
Figure 3.5.	Graph of the difference between microphone distances (d_1-d_2) versus the difference in propagation time sensitivity.....	36
Figure 3.6.	Picture of the α -prototype.....	37
Figure 3.7.	Description of the electronic signals test done using the speaker from the α and β -prototypes.....	38
Figure 3.8.	Picture of the β -prototype test bed.....	39
Figure 3.9.	Wiring diagram of the microphone system (left) and microphone measurement circuit (right).....	40
Figure 3.10.	A wiring diagram of the system that controls the linear actuator movement.....	41

Figure 3.11.	A wiring diagram of the system that monitors the current drawn by the linear actuators.....	42
Figure 3.12.	LabVIEW block diagram representation of the functions used to generate the audio signal.....	44
Figure 3.13.	LabVIEW block diagram representation of the functions used to acquire the audio signal.....	45
Figure 3.14	LabVIEW block diagram representation of an example script that monitors the current given to the actuator, the corresponding force, and stops the motion of the actuator based on the force reading.....	46
Figure 3.15.	Amplitude of the device in decibels across the upper end of the audible frequency spectrum outlining the device safety.....	47
Figure 4.1.	Plots of the expected phase shift of the system.....	50
Figure 4.2.	LabVIEW block diagram representation of the VI used to acquire signal and compute the frequency and phase.....	51
Figure 4.3.	Q-Q plot of the expected frequency versus the measured frequency.....	52
Figure 4.4.	Measured phase shift between two signals across the phase and frequency range.....	53

Figure 4.5.	σ_t/f across the frequency range of interest.....	54
Figure 4.6.	σ_p/f across the frequency range of interest.....	54
Figure 4.7.	Phase variance between the measured and expected phase shift across the frequency range.....	55
Figure 4.8.	Calibrated measured phase shift between two signals across the phase and frequency range.....	56
Figure 4.9.	Injection of high frequency noise from the AC/DC converter.....	57
Figure 4.10.	Method flow diagram of the microphone and speaker coupling force experiment (A) and picture of the test setup (B).....	60
Figure 4.11.	A plot of the calibration curves relating physical load applied during actuator extension and current load on the DC motor within the actuator.....	62
Figure 4.12.	A plot of the calibration curves relating physical load applied during actuator extension and the extension speed of the linear actuator.....	62

Figure 4.13. A plot of the calibration curves relating physical load applied during actuator extension and current load on the DC motor within the actuator.....64

Figure 4.14. A plot of measured current regulated by a series resistor value of 0 Ω with no load, 100 Ω , 80 Ω , and 0 Ω with maximum load. At the 0 Ω conditions, no load indicates the actuator was not stopped by the tester, and max load indicates the actuator was stopped by the tester. The series of the plot (gray, red, blue, green) indicate the predicted current value.....66

Figure 4.15. LabVIEW block diagram representation of script used during the software timed distance experiment.....68

Figure 4.16. Method flow diagram used in the software timed distance measurement experiment where the actuator distance of the actuator pushing a known load is measured.....69

Figure 4.17. Q-Q plot of the expected distance versus the measured distance in inches (in.) for the software-timed distance measurement experiment.....70

LIST OF EQUATIONS

Equation 2.1. Bar wave equation.....	18
Equation 2.2. Phase shift (in degrees) as a function of frequency and time delay (in seconds).....	20
Equation 3.1. Velocity of a sound wave as a function of distance, propagation time, elastic modulus, and density.....	30
Equation 3.2. Velocity of sound propagating through bone as a function of bone thickness and bone propagation time.....	30
Equation 3.3. Sound propagation time through bone as a function of bone thickness elastic modulus, and density (Computation governing equation).....	30
Equation 3.4. Bone density sensitivity function.....	33
Equation 3.5. Bone thickness sensitivity function.....	33
Equation 3.6. Elastic modulus sensitivity function.....	34
Equation 3.7. Difference in propagation time as a function of the difference between two governing equations.....	35
Equation 3.8. Microphone position sensitivity function.....	35
Equation 4.1. Root mean square relative error (RRMSE).....	52
Equation 4.2. Arduino current calculation.....	59

1. INTRODUCTION

1.1. Background

Osteoporosis is a medical condition in which there is a progressive degradation of bone tissue that correlates with a characteristic decrease in bone density (BD). A reduction in BD limits the skeletal systems' ability to provide structure, protect internal organs, and allow movement. Populations most at risk for developing osteoporosis include post-menopausal women, diabetic patients, and the elderly, representing a large population within the State of Maine. In the United States (US), there is mounting evidence of an increasing prevalence of osteoporosis and fragility fractures.¹ This is alarming due to the reported increase in absolute mortality for at-risk populations within one year of a fragility fracture. Early identification and intervention in cases of osteoporosis are thought to improve prognosis giving rise to bone densitometric and sonometric diagnostic specialties.¹

Current densitometric (x-ray) and sonometric (sound) devices used to monitor bone health include quantitative computed tomography (QCT), dual-energy x-ray absorption (DXA), and ultrasound (QUS). These devices are used by healthcare providers to help diagnose bone diseases. All methods are expensive and, in the cases of QCT and DXA, patients are exposed to small, frequent doses of ionizing radiation. While these methods can effectively measure BD, they are critically limited for applications in rural healthcare because they are cost-prohibitive to rural medical facilities and to patients that require routine screening. The diversity of at-risk patient populations and current expensive and invasive BD devices drives the need for a rapid, low-cost, and non-invasive approach to identifying, monitoring, and improving the intervention timeline for pathologies related to BD deficiencies.

1.2. Thesis Objectives

The present work proposes the use of audible sound as a potential solution that could safely and effectively measure BD by minimizing cost drivers and increasing device simplicity to improve availability. This work aims to evaluate the feasibility of using TDS as a potential method to assess bone health, suggest potential pathways to the commercialization of such a device, and make recommendations for future work.

1.3. Thesis Layout

Chapter One introduces the current work. Chapter Two discusses all background information relevant to the current work including current bone diagnostic specialties and their application in rural and global health settings, osteoporosis, the physics of sound, TDS, and potential pathways to commercialization. Chapter Three describes the test bed that was constructed and will serve as an instrument for future research on the interaction between audible sound and bone structure. Chapter Four presents the experiments and methods used to assess the performance of the test bed. Chapter Five lists and discusses recommendations for future work.

2. LITERATURE REVIEW

2.1. Introduction

Osteoporosis is a medical condition in which there is a progressive degradation of bone tissue that correlates with a characteristic decrease in BD.¹ A reduction in BD limits the skeletal system's ability to perform critical functions and puts the affected bones at risk of fracture. Osteoporosis is the most common bone disease in humans affecting over 200 million people globally and is responsible for approximately 8.9 million fractures annually.² Populations most at risk for developing osteoporosis include *post-menopausal* women, diabetic patients, and the elderly, which represent a large population within the state of Maine. In the US, there is mounting evidence of an increasing prevalence of osteoporosis and fragility fractures. This is alarming due to the reported increase in absolute mortality for at-risk populations ranging from 9.4% - 32.3%, dependent upon gender and fracture site, within one year of a fragility fracture.³ Fragility fractures occur when a bone is weakened by an illness or disease and breaks because of low-energy trauma (e.g., falls from standing height or less). Low energy requirements for bone breaks mean that daily activities can be dangerous for people with osteoporosis. Early identification and intervention in cases of osteoporosis are thought to improve prognosis giving rise to bone densitometric and sonometric diagnostic specialties.

2.2. Bone Diagnostic Specialties

Bone diagnostic devices can be categorized into two diagnostic specialties; bone densitometry, and bone sonometry. These specialties are further described in their respective sections. Specialties exist because of differences in the information gathered about bone structure and their methods of acquisition. Perhaps the most significant difference in information gathered is the measurement of areal (e.g., g/m^2) and volumetric (e.g., g/m^3) BD. Areal and volumetric

density are often grouped under the term “BD” likely because they have been reported as equally accurate and sensitive in predicting the strength of bones which is important when assessing overall bone health and risk of fracture.⁴ The US Food and Drug Administration (FDA) recognizes both bone densitometry and sonometry under their Code of Federal Regulations Title 21. Although each of the methods has been proven to assess BD and diagnose diseases related to low BD such as osteoporosis and low bone mass (osteopenia), DXA is considered the densitometric gold standard due to the specificity provided by the test.^{5,6} Recently, there is growing evidence to support that DXA may not be as clinically applicable for older adults with diabetes.⁷⁻⁹ Concerns over the effectiveness of diagnostic tests for at-risk patient populations suggest a new method is needed for monitoring bone health.

2.2.1. Osteoporosis

Osteoporosis is a medical condition in which there is a progressive degradation of bone tissue that correlates with a characteristic decrease in BD.^{1,10-13} During normal human growth and development, the rate of bone formation is greater than the rate of bone resorption inducing a positive remodeling balance. As a result, human bones form and develop. With osteoporosis, bone homeostasis is disrupted. Bone homeostasis disruption refers to a state where bone resorption by osteoclasts happens at a faster rate than bone matrix formation by osteoblasts. This is known as a negative remodeling balance.¹³ In cases of negative remodeling balances, changes in the bone structure are reflected in BD. In Figure 2.1, scanning electron micrographs (SEM) of normal and osteoporotic bone biopsies are

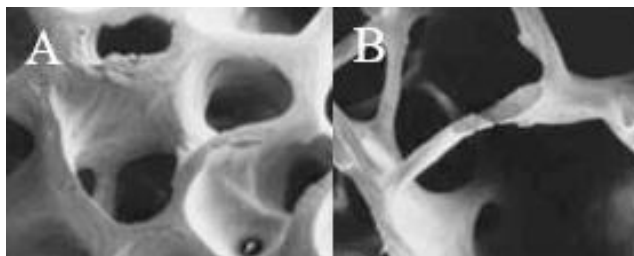


Figure 2.1. SEM image of normal (A) and osteoporotic bone (B). Reproduced from ref (17).

shown which outline their difference in density. The change in density is dependent upon the porosity of the bone structures which in a healthy human ranges from 40 - 92% porous with an average pore size from 0.64 - 0.85 mm, dependent upon the location of the bone.¹⁴⁻¹⁶ The change in porosity and resulting reduction of density associated with osteoporosis decreases the strength of the bone and increases the likelihood of fracture. The onset of osteoporosis is preceded by low-bone mass, formerly known as osteopenia. The likelihood of preventing the onset or severity of osteoporosis is through early identification and treatment.

Osteoporosis is caused by several factors related to bone health such as diet, exercise, hormones, and genetics. Deficiencies in calcium, vitamin D, and phosphate are the most common dietary causes seen and disrupt the bone mineralization process. Since bone is mechanoresponsive, meaning that the more exposure to load the denser it becomes, exercise is critical to maintaining proper bone health. Osteoporosis is also commonly associated with the aging process.¹⁰ Figure 2.2. shows the relationship between BD and time among males and females. The remarkable difference between males and females is the rapid decline in BD due to hormonal changes associated with menopause in women.¹⁷

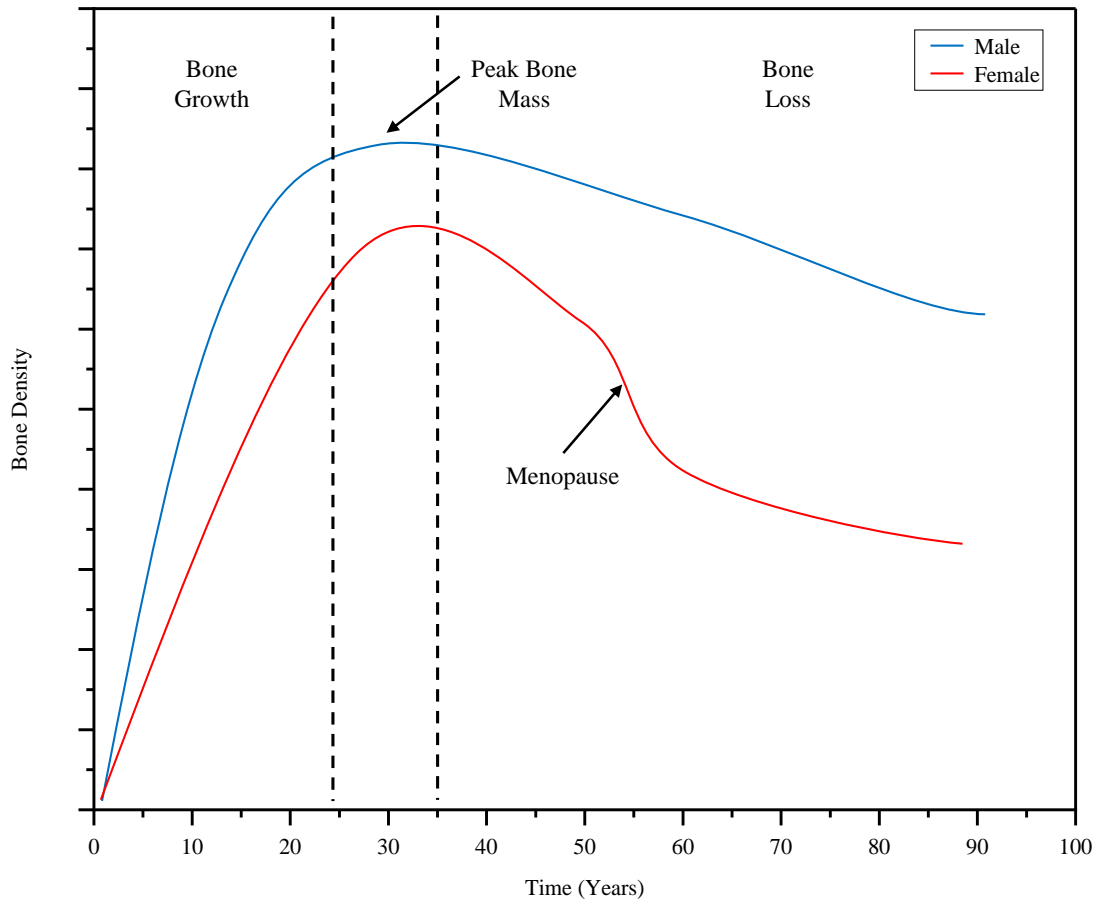


Figure 2.2. Representation of BD over time in male and female populations.

Groups most at risk for osteoporotic degradation include patients with type 1 diabetes mellitus (T1DM), geriatric (elderly) patients, astronauts, and post-menopausal women drawing the attention of a variety of national and international health authorities including NASA, the National Institute of Health (NIH), and the World Health Organization (WHO).^{8,17-19} Patients with T1DM are at an increased risk of developing osteoporosis for several different reasons including osteoclast up-regulation and osteoblast down-regulation.¹⁹ Geriatric patients and postmenopausal women are at an increased risk of developing osteoporosis because of changes in hormones such as testosterone and estrogen that occur as humans age evident in Figure 2.2. The Office of Disease

Prevention and Health Promotion (an office of the US Department of Health and Human Services) estimates that the US has 10.2 million people aged 50 years and older who have osteoporosis with an additional 43.4 million people with low bone mass (formerly osteopenia). Women represent 80% of this population while men represent 20%.¹² Astronauts represent a small section of those at risk for osteoporosis because they are exposed to less load (less gravity) during their time in space. The types of bone assessments used for at-risk populations can vary based on regulatory guidelines generated nationally and internationally and adopted at medical facilities. Common guidelines include those created by the U.S. Preventative Services Task Force (USPSTF), the International Society for Clinical Densitometry (ISCD), and the WHO.^{1,20,21}

2.2.2. Bone Densitometry

Bone densitometry is a clinical field of study used to assess bone health by monitoring BD. Within this field, bone densitometers are used as the primary medical device to measure and assess BD. The FDA defines a bone densitometer as a medical device that uses X-ray or gamma-ray transmission to measure BD and mineral content. These devices typically include patient and equipment supports, signal analysis and display equipment, parts, and other related accessories.²² The global bone densitometer market size has been estimated at \$299 million in 2022 by MarketsandMarkets Research Private Ltd.©, a global market research company, and is expected to grow at a compound annual rate of 4.7% over the next five years.²³ These estimations can be accredited to the increase in healthcare expenditures related to overall health and wellness in addition to the increase in osteoporosis prevalence. Examples of densitometer techniques include dual-energy X-ray absorption (DXA) and quantitative computed tomography (QCT) because of their use of X-rays to assess bone quality.

2.2.2.1. Dual-Energy X-ray Absorption (DXA)

DXA is an attenuation-based method of measuring BD using X-rays. DXA uses two different X-ray energies to create a two-dimensional (2D) image of the bone structure. The use of two different energy levels improves the device's ability to distinguish between the bone structure and surrounding soft tissue. Figure 2.3. shows an image of the Lunar iDXA scanner, and an image of the test results provided. Bone is known to absorb X-rays and appears white within the generated image.²⁴ The absorbance is quantified by measuring the change in radiation energy per pixel at specific imaging sites.²⁵ The most common imaging sites are the femoral head and the lumbar spine because they are the primary load-bearing bones for the human skeleton.^{21,26,27} Daily calibration is often required for most types of DXA scanners to assure the quality of the results.²⁸ In these cases, calibration phantoms are used that mimic the material properties of bone. Calibration phantoms generally range in densities across the clinically relevant range (0.7 – 1.5 g/cm²) and are specific to each manufacturer.²⁹ This means that cross-calibration is required between systems to effectively compare results.²⁸ Commonly, the phantoms are composed of hydroxyapatite (HA) and shaped like relevant bone structures. The results of a DXA scan include a T-score and Z-score comparing the results of the density test to normative reference populations, generally based on age. The ability of DXA tests to distinguish between the bone structure and surrounding soft tissue makes DXA scans the preferred method of assessing BD as recommended by the ISCD and WHO.^{1,21}

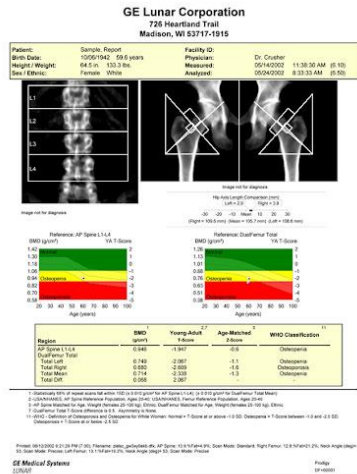


Figure 2.3. Report of a DXA scan of the hips and spine (left) scanner and the GE Healthcare Lunar iDXA scanner (right). Adapted from ref (24).

2.2.2.2. Quantitative Computed Tomography (QCT)

QCT is a method of measuring trabecular BD using X-rays.³⁰ QCT introduces x-rays of the same energy level at different angles around the body to create cross-sectional images of the bone. An image of the GE GoldSeal Optima CT660 device and corresponding 2D test image is shown in Figure 2.4.^{30,31} QCT devices can build 2D and three-dimensional (3D) images of bone to assess quality, generally of the spine and proximal femur. 3D images are more commonly used to

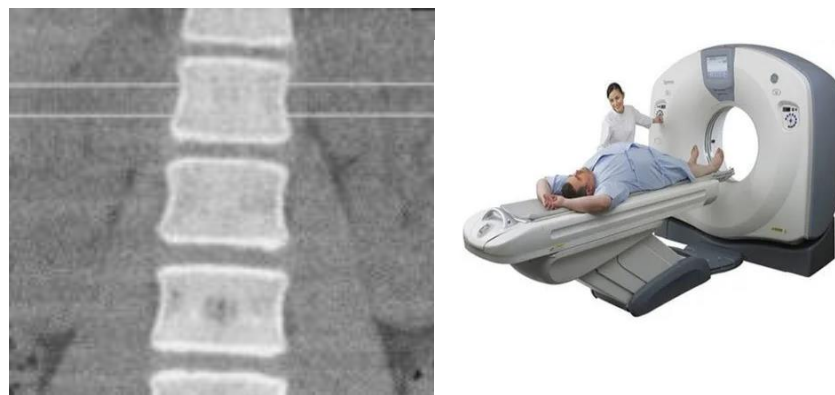


Figure 2.4. Anterior 2D QCT scan of the human spine reproduced from ref (30) (left) and GE GoldSeal Optima CT660 QCT scanner (right) adapted from GE Health ref (31) (right).

estimate bone strength through finite element analysis (FEA) and X-ray attenuation.^{32,33} 2D images are more common and are created via a two-step process. The first step consists of a scan to acquire data and the second step creates the 2D image using tomographic reconstruction.^{18,30} The tomographic image reconstruction is based on the X-ray absorption coefficients acquired during the primary scan which are dependent on the type of tissue the X-rays pass through. CT numbers are computed based on the X-ray attenuation of water and are given in Hounsfield units (HU).³⁰ Hounsfield units can then be converted to a volumetric density of the units milligrams per cubic centimeter (mg/cm^3) based on a calibration procedure using a calibration phantom.^{18,30} Calibration phantoms are specific to each device meaning that they cannot be used between devices unless there is a secondary calibration completed comparing the two existing phantoms. It is common for QCT calibration phantoms to use a range of volumetric (50, 100, 200 mg/cm^3) and areal (0.5, 1.0, 1.5 g/cm^2) densities to represent the properties of bone within the anatomic region of interest (ROI). HA is generally used to represent bone while tissue-equivalent plastics are used to represent the material main body.³⁴ Similar to DXA, the results of a QCT scan include a T-score and Z-score to compare the results of the BD test to a normative reference population, although the ISCD cautions the comparison of statistical results between QCT and DXA.

2.2.2.3. Radiation

One of the biggest concerns associated with DXA and QCT is that both techniques use ionizing radiation. This concern is validated through years of focused research showing that high doses of ionizing radiation damage human cells and disrupt metabolic processes.³⁵ Although there are no official limits on the number of densitometric tests, the ISCD recommends that BD tests should not be taken more frequently than once every one to two years.²¹ QCT exposes patients to an effective dose of 5 – 10 mrem per scan while DXA exposes patients to a much lower effective dose of 0.1 – 1.8 mrem per scan.³⁶ Both the effective doses for QCT and DXA are heavily debated and dependent on the type of device and scan performed. The US Nuclear Regulatory Commission (NRC) does regulate the occupational dose limits that are shown in Table 2.1.³⁷ The establishment of occupational dose limits is also one of the main cost drivers associated with densitometric

techniques as these devices require significant infrastructure investments to house the equipment safely. Large hospitals can more easily accommodate the space and cost of using these devices safely while small and rural hospitals struggle to do the same.

Table 2.1. US Nuclear Regulatory Commission (NRC) occupational dose limits. Reproduced from ref (37).

NRC Occupational Dose Limits	
Whole Body	5,000 mrem/year
Any Organ	50,000 mrem/year
Skin	50,000 mrem/year
Extremity	50,000 mrem/year
Lens of Eye	15,000 mrem/year
Embryo/Fetus	500 mrem/year
Member of the Public	100 mrem/year

2.2.3. Bone Sonometry

Bone sonometry is a clinical field of study used to assess bone health by monitoring the acoustic properties of bone. Unlike densitometric techniques, sonometric techniques use ultrasound eliminating the need for ionizing radiation. The FDA defines a bone sonometer as a

medical device that uses ultrasound energy to measure acoustic properties of bone that indicate overall bone health and risk of fracture. These devices typically include a voltage generator, a transmitting transducer, a receiving transducer, and hardware and software for the reception and processing of the received ultrasonic signal.³⁸ Examples of sonometer techniques include broadband ultrasound attenuation (BUA) and speed of sound measurements (SOS). The bone sonometer market has been estimated at \$9.8 billion in 2020 by Expert Market Research, a global market research company.³⁹ Over the next five years the compound annual growth rate of the bone sonometer market is estimated at 9.0%, which is a greater growth rate than the bone densitometer market (4.7%) and the medical device market (5.0%).

2.2.3.1. Quantitative Ultrasound (QUS)

QUS is a method of assessing bone health that generally uses ultrasonic frequencies ranging from 0.5 - 1.5 MHz.^{40,41} While QUS does not directly measure BD, QUS measures the speed of sound (SOS) and broadband ultrasound attenuation (BUA) to calculate a stiffness index (SI) of the bone structure. Figure 2.5. shows a picture of the GE Lunar Achilles ultrasound device and corresponding test results.⁴¹ Most QUS devices are used to test the calcaneus because it is



Figure 2.5. Report (left) generated from a heel assessment using the GE Lunar Achilles ultrasound device (right). Adapted from ref (39).

relatively uniform in its composition at greater than 90% trabecular bone with the surrounding soft tissue representing a small amount (~13%) of the heel's total thickness.^{26,42-44} The method of measuring SOS and BUA varies between devices.²⁶ Common methods of measuring the speed of sound include limb velocity, where the velocity of ultrasound is calculated based on the total heel thickness and total sound propagation time; bone velocity, where the velocity of ultrasound moving through bone is calculated based on the thickness of bone and propagation time through bone thus excluding soft tissue; and time-of-flight velocity, where the velocity of sound is calculated based on the differences in ultrasound propagating through water and the heel.²⁶ Other descriptions of velocity that are used to differentiate between devices describe the ultrasound signal. These descriptions include phase velocity (the velocity of a single frequency component as a function of frequency), group velocity (the velocity of a centralized pulse), and signal velocity (the velocity of the leading edge of a pulse).⁴⁵ Differences in attenuation between devices arise from different calibration phantoms. QUS uses gels to couple the transducers to the human body to match the acoustic impedance of the surrounding soft tissue.⁴⁶ Similar to densitometric techniques, QUS devices compute a T-score and Z-score to compare the results of the BD test to a normative reference population. The ISCD recommends that these results not be compared to the results of densitometric techniques.²¹

2.2.4. Bone Densitometric/Sonometric System

The densitometric/sonometric system (DSS) is a system within clinical healthcare that is responsible for assessing bone health using X-ray or sound, respectively. Figure 2.6. outlines this system from left to right. Like any quality healthcare system, the DSS begins with a patient. This patient likely has a health issue related to their bone structure or is a part of a high-risk category. In rural areas like Maine, the patient is then either going to visit a major hospital or a rural hospital or clinic for an assessment. In the rural facility, the testing equipment is generally limited to QUS if the facility has access to any equipment at all. This means that the patient likely requires a second visit to a major hospital for evaluation. At the major hospital, the patient is likely to have access

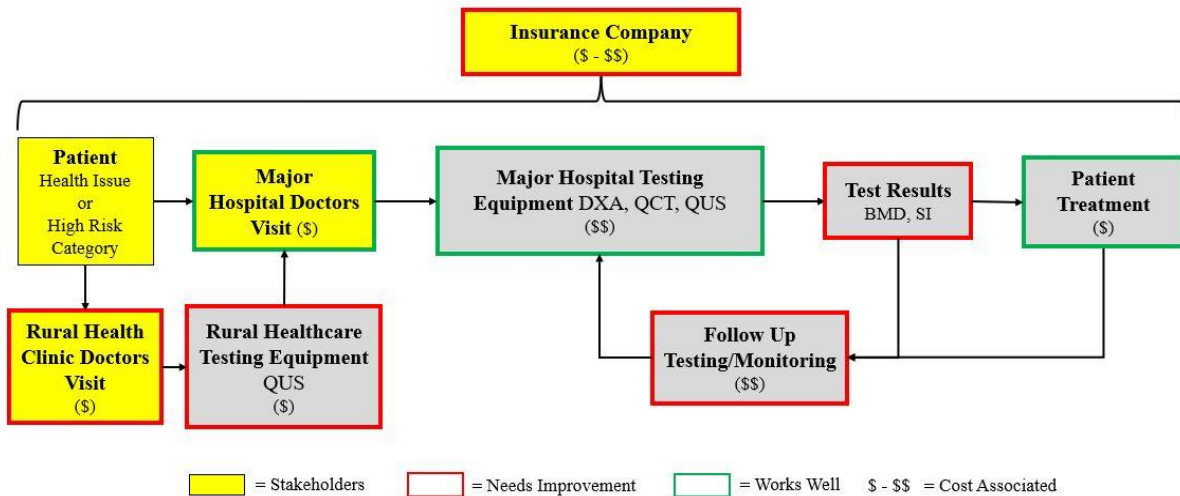


Figure 2.6. System map of the densitometric and sonometric system.

to DXA, QCT, and QUS. After testing, the patient will get their test results and healthcare providers will make a diagnosis and recommend treatment. The patient will then be required to have follow-up testing and monitoring done to ensure the treatment is effective and the patient is improving. From here, the system enters a cycle of testing and treatment until the provider thinks

it is no longer medically necessary to evaluate the patient's bone health. Insurance companies regulate the DSS because they control which tests will be covered by insurance.

The yellow boxes in Figure 2.6. represent the stakeholders within the DSS. Stakeholders are broadly defined as individuals who have an interest in the way the system performs or operates. The areas highlighted in green represent areas where the current system works well. At major hospitals, patients have access to all forms of densitometric and sonometric assessments. This bodes well for the proper diagnosis of patients because some tests are thought to be more appropriate for different patient populations.⁷⁻⁹ The treatment of patients is an area of the system that works well because many approaches work well to treat bone diseases such as osteoporosis.⁴⁷ The areas highlighted in red represent areas where the current system needs improvement. In other words, these areas present opportunities for innovation. Innovation within a rural hospital or clinic would improve the availability of bone health assessments by reducing all associated costs. Other improvements in the testing system would be a standardization of results and improved safety for follow-up testing that is problematic for approaches that use ionizing radiation. Insurance companies have also been identified as an area of improvement because they represent an entity that regulates tests that are given to patients. At present, there is likely little to be improved within this area of the system, but it is important to understand what tests and devices insurance will cover when addressing problems in other areas.

2.2.5. Recommendations for Bone Health Assessments in Rural and Global Health Applications

Creating tests that can be used in resource-constrained settings is becoming a focal point for the improvement of rural and global healthcare. This led to the development of ASSURED criteria by the WHO. ASSURED stands for affordable, sensitive, specific, user-friendly, rapid and robust, equipment-free (i.e. requiring no additional equipment), and deliverable.⁴⁸ Based on the ASSURED criteria, Figure 2.7. was generated to compare device price, size, single-use safety, prolonged-use safety, ability to assess bone health, and ability to predict osteoporotic fracture of QCT, DXA, and QUS. The specifics surrounding the device price, size, safety, ability to assess bone health, and predict osteoporotic fracture are found in Table A.1. The red areas for Figure 2.7. represent regions where the device performs poorly indicating that there is room for major

Method	Device Price	Device Size	Device Safety (Single Use)	Device Safety (Prolonged Use)	Assess Bone Health	Predictor of Osteoporotic Fracture
QCT	High	Large	Moderate	Low	High	Moderate
DXA	High	Large	Moderate	Low	High	High
QUS	Moderate	Medium	High	High	High	Moderate

■ = Optimal ■ = Okay ■ = Bad

Figure 2.7. A heat map that was generated to evaluate the current methods of assessing bone health from a rural and global health initiative prospective.

improvement. Yellow areas represent regions where the device performs relatively well indicating room for improvement. Green areas represent regions where the device performs optimally indicating little to no room for improvement. While QCT, DXA, and QUS can all effectively assess bone health, QUS is favored in price, size, and safety. This shows that QUS is the best choice for resource-constrained settings, but there is an opportunity to improve the device price, size, and

ability to predict osteoporotic fracture which could be achieved by significantly changing aspects of current QUS devices.

2.3. Physics of Sound

Sound or acoustic waves are commonly defined as mechanical disturbances through an elastic medium.⁴⁹ Solids, liquids, and gases are all examples of elastic mediums that conduct sound. The speed at which sound propagates through a material is dependent on the density of the material, which is why sound propagates the fastest through solids, followed by liquids, and finally gases. The relationship between the speed of sound and the density of solids is shown in Figure 2.8.

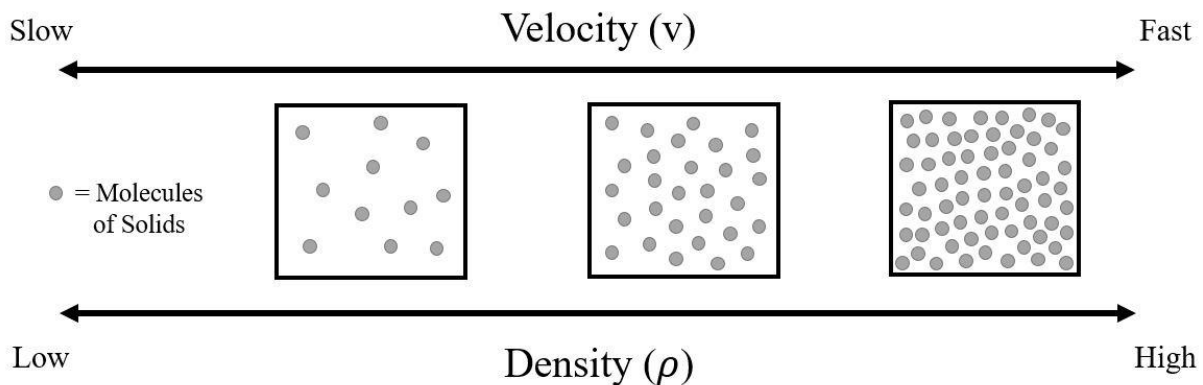


Figure 2.8. A simplified diagram showing that the velocity of sound is the fastest in dense solids and slower in less dense solids.

Sound waves can exist as both transverse and longitudinal waves in solids.⁵⁰ The type that is present is dependent upon the method of generation.⁴⁹ With common speakers, longitudinal waves are generated from a vibrating diaphragm in the form of pressure waves that oscillate along the direction of propagation. Amplitude, frequency, and phase are all common ways to describe wave propagation, but sound is classified by frequency. Infrasound, audible sound, and ultrasound are three types of sound. Their respective frequency ranges are shown in Figure 2.9. Although each

frequency level of the sound spectrum has clinical applications, ultrasound is the most popular for assessing bone health.

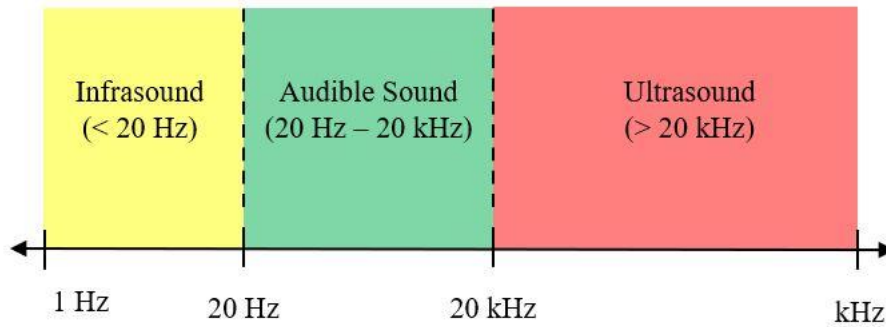


Figure 2.9. Sound spectrum identifying the frequency ranges of infrasound, audible sound, and ultrasound.

Although ultrasound is now commonly used to assess bone health, the physics behind the interaction of sound with trabecular bone is still debated.⁴⁵ This debate is largely due to the structural organization and composition of bone discussed in the next section. A common concern with sound base measurements in solids is related to sound's dispersive nature. In trabecular bone, dispersion is considered negligible.⁵¹ Although complex methods of modeling sound propagation through trabecular bone have been developed, bar wave theory is effective in predicting the speed of sound at low frequencies where the wavelength is much greater than the pore size and lateral dimension.⁴⁵ This case is especially true within the audible and infrasound spectrum. The bar wave equation is shown in Equation 2.1. where the velocity of sound (v) is given as a function of material elastic modulus (ϵ) and density (ρ).

$$v = \sqrt{\epsilon/\rho} \quad (2.1.)$$

2.4. Bone Structure

Bone is a hierarchical structure meaning that there are tiers of rank dependent upon the size scale. The four primary size scales are shown in Figure 2.10.¹⁵ At the sub-nanostructure, collagen molecules (1.5 nm in diameter), are combined with HA crystals forming collagen fibrils (0.5 μm in diameter) that exist at the nanostructure. The collagen fibrils are arranged in a lamellar pattern forming the osteon (100 μm in diameter), which is the structural unit of bone. Each osteon is composed of a central canal, peripheral canals (lamellae) that contain nerves and vasculature, and holes (lacunae) containing the osteocytes. At the macrostructure scale the porous trabecular (or cancellous) bone is surrounded by the cortical (or compact) layer. Trabecular bone is a porous structure at approximately 40 – 92% porous composed of trabeculae and marrow-filled cavities.^{14–16,52} Conversely, compact bone is less porous at approximately 3 – 12% porous.¹⁵ Recognizing the substructures of bone is important as it dictates properties of interest such as density and elastic modulus seen at the macrostructure level.

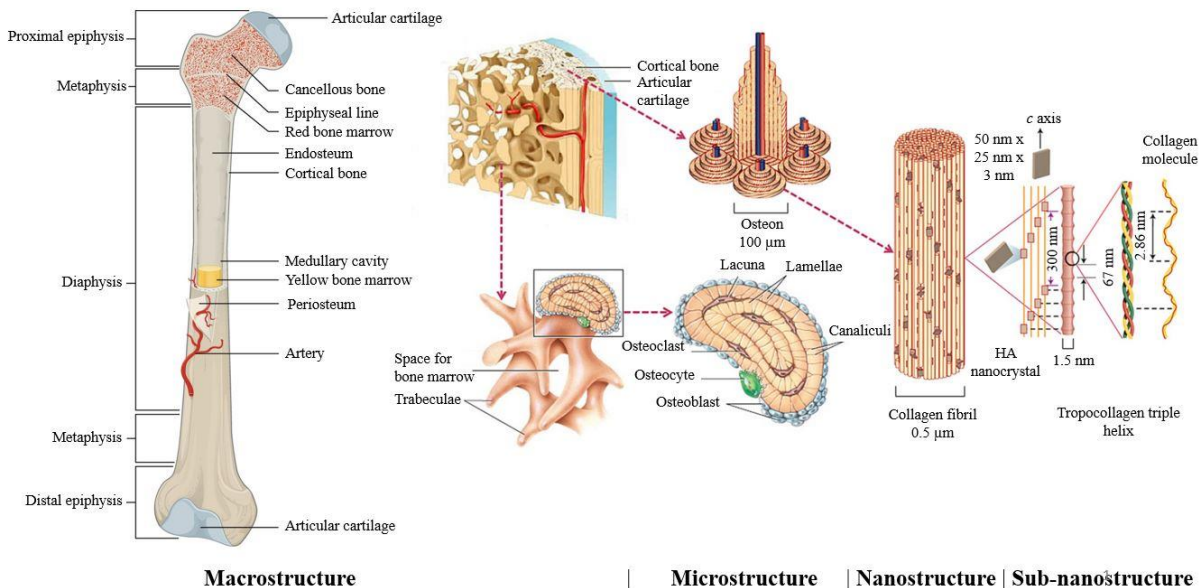


Figure 2.10. Shows the bone hierarchy from the macrostructure to the sub-nanostructure. Adapted from ref (15).

2.5. Time Delay Spectroscopy (TDS)

TDS is used to describe the time between events. In this work, events refer to the difference between two generated signals. Figure 2.11. illustrates this as the difference in time (Δt) between

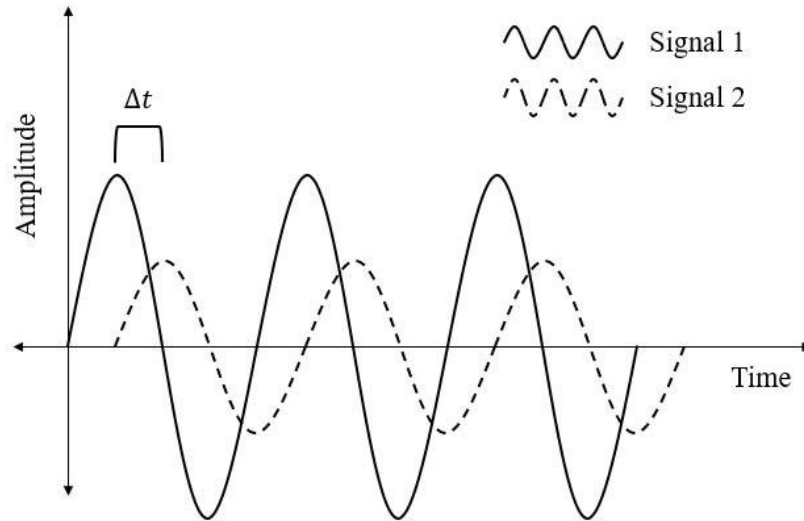


Figure 2.11. Application of TDS on two arbitrary signals 1 and 2 of the same frequency.

the peaks of two signals of the same frequency. Other common reference points include troughs and zero-crossings. The time difference between the two signals can also be described as the phase difference of shift in degrees or radians which relates to a time difference. The phase shift between two waves can be calculated by measuring and taking the difference between the individual phases. Common methods of calculating phase include a Fourier Transform method, zero-crossing method, and peak detection method. Equation 2.2. gives the phase shift (ps) of a wave as a function of frequency (f) and time delay (td).

$$ps = 360(f)(td) \quad (2.2.)$$

For TDS to be effective, the length of a single incident wave period (cycle) must be greater than the anticipated phase shift. Figure 2.12. shows a graph of the minimum and maximum recorded speed of sound through bone across the North American minimum and maximum heel

thickness.⁴³ The speed of sound used in this calculation is based on the speed of ultrasound since measurements with audible sound have not been reported. In Figure 2.12., the green region represents areas where this condition is satisfied while the red region represents where the is not satisfied. Much of the green region is occupied by the audible sound spectrum while the red region captures the range of frequencies where clinical ultrasound exists. This means that audible sound is the logical selection for the application of TDS.

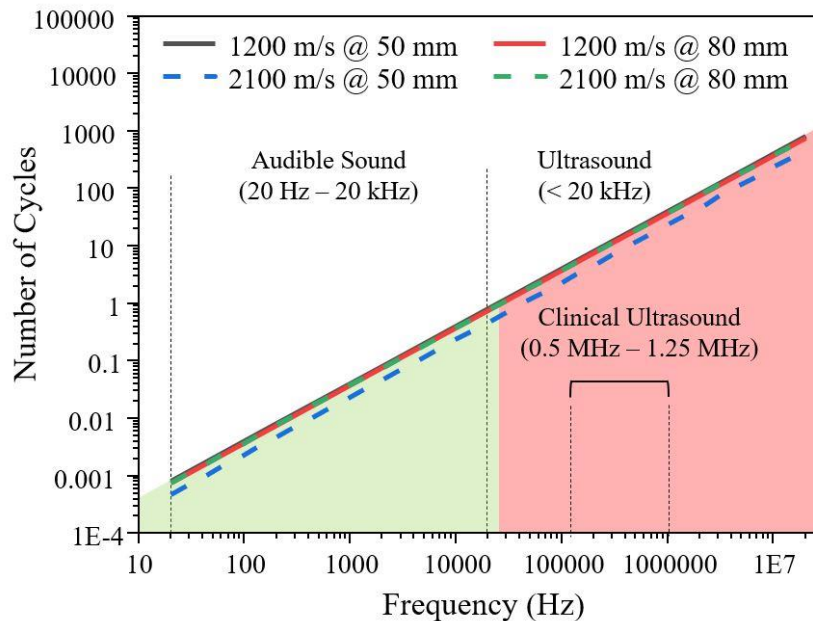


Figure 2.12 . A graph plotting the minimum and maximum recorded speeds of ultrasound (used to estimate the behavior of audible sound) across the minimum and maximum North American heel thickness.

2.6. Prospective Markets

In 2021, the global medical device market size was estimated at \$488.98 billion and is expected to increase at a 5.0% compound annual growth rate over the next eight years.⁵³ In 2020, the same growth rate of 5% was projected in the US medical device market which accounts for roughly 36% of the global market – estimated at 176.7 billion.⁵⁴ The size of the global and national

medical device market can be attributed to the variety of products offered within the market itself. The World Health Organization (WHO) defines a medical device as,

“ . . . all the health technologies (except for vaccines and medicines) required for prevention, diagnosis, treatment, monitoring, rehabilitation, and palliation. They are indispensable for universal health coverage, monitoring wellbeing, and addressing outbreaks or emergencies”

The WHO subcategorizes the medical device market into single-use devices, implantable, imaging, medical equipment, software, in vitro diagnostics, surgical and laboratory instruments, and personal protective equipment. Similarly, a U.S. Medical Device Manufacturers Market Report for 2021 – 2028 published by Grand View Research© (a market research and consulting firm based in San Francisco, California) divided the medical device market into four major categories: diagnostic imaging, consumables, patient aids, orthopedics, and others. Diagnostic imaging and orthopedics combined accounted for ~50% of the total medical device market size in the US. Evaluating the current size and projected growth of the global, national, diagnostic imaging, and orthopedic medical device market shows a substantial market for the proposed device.

It is estimated that osteoporosis affects over 200 million people globally and is responsible for approximately 8.9 million fractures annually.² A 2022 study on the global market for osteoporosis testing reflects the growing prevalence by projecting a total market compound annual growth rate (CAGR) of 6.2%, reaching a total market value of \$504 million by 2027.² According to the WHO ASSURED criteria for identifying the most appropriate diagnostic tests for resource-constrained settings, the proposed device could also be categorized within the point-of-care (POC) market.⁴⁸ This market is estimated to grow at a CAGR of 10.1% and reach a \$73.9 billion valuation

by 2028.⁵⁵ The prevalence of osteoporosis, significant growth of relevant markets, and alignment of project goals with WHO criteria outline a plausible pathway to marketability.

2.7. Fourt-Woodlock Sales Forecast

A more specific forecast of the revenue generated by a device that uses audible sound to measure BD can be calculated using the Fourt-Woodlock Sales Forecast. This technique calculates the revenue generated in the first year of trial sales which is the sum of the trial and repeats sales of the product. Trial sales are a product of the number of final decision makers or people that might buy the product, the percentage of those people that can be made aware that the product exists, the percentage of people that have access to the product, the percentage of people that can be persuaded to use the product, and the cost of the first purchase of the product. Repeat sales are like trial sales but replace the first purchase revenue with the repeat purchase rate, the repeat purchase revenue, and the number of repeated purchases. For this work, moderate models of two potential devices were created.

The first model is for a clinical device that uses audible sound to rival DXA, QCT, and ultrasound. This device would be used in hospitals and rural health facilities alike. This means that the device would likely be used by a combination of primary care providers, podiatrists, and orthopedic surgeons. In the US, there are an estimated 294,834 primary care providers, 18,000 podiatrists, and 22,965 orthopedic surgeons for a total of 335,799 possible customers.⁵⁶⁻⁵⁸ Of these customers, an estimated 2% can be made aware of the product, 100% will have access to purchase the product, and 0.5% will be persuaded that the technology is better than DXA, QCT, or ultrasound. These estimates were based on “Fundamentals of Innovation for Researchers Week 6”.⁵⁹ The cost of the device is estimated at \$1,000, representing a 50% price reduction compared

to a used QUS device. Assuming there will be no repeat sales, the first-year sales are estimated at \$33,579.90 (~33 devices).

The second model is a device that is used in the homes of patients to monitor bone health. This device would be like pulse oximeters or blood pressure cuffs that are commonly used in hospitals but can also be purchased at local stores. This means that the likely customers will be people who have osteoporosis or low bone mass (osteopenia). In the US, an estimated 10.2 million people had osteoporosis and another 43.3 million had low bone mass giving a total of 53.6 million potential customers.⁶⁰ Of these customers, an estimated 1% can be made aware of the product, 100% will have access to purchase the product, and 1% will be persuaded that the technology is beneficial to monitor their bone health. Like the first model, these estimates were based on “Fundamentals of Innovation for Researchers Week”.⁵⁹ The cost of the at-home device is estimated at \$20, which is a low estimate that is competitive with at-home testing devices. Assuming there will be no repeat sales, the first-year sales are estimated at \$107,000 (~5,350 devices).

2.8. Food and Drug Administration (FDA) Approval Process for Medical Devices

The Food and Drug Administration (FDA) classifies medical devices to ensure safety and effectiveness.⁶¹ These classifications are based on the risk associated with the device and the regulatory processes required to make using them safe. Each device is categorized into one of three classes, Class I, II, or III, based on a risk assessment. Class I devices pose the lowest risk and present minimal potential for harm. Examples of Class I medical devices include stethoscopes, bandages, surgical masks, and tongue depressors. Class II devices pose a moderate risk with a greater potential for harm than Class I. Examples of Class II medical devices include catheters, surgical gloves, bone sonometers, and contact lenses. Class III devices pose the greatest risk because they are used to sustain or support life, implanted, or present a potentially unreasonable

risk of illness or injury. Examples of Class III medical devices include pacemakers, ventilators, and implanted prosthetics.

After a preliminary classification by the device manufacturer, a submission or exemption must be filed and approved by the FDA before the sale of the medical device. These submissions and exemptions include a 510(k), 510(k) exemption, and De Novo. A premarket submission 510(k) is made to the FDA to demonstrate that a device is safe and effective. The safety and effectiveness are based on substantial equivalence which means that the new device is as safe and effective as an existing device. The existing devices are known as the predicate. The FDA states that a device is substantially equivalent to a predicate if the device has the same intended use as the predicate and has the same technological characteristics. Substantial equivalence can also be reached by having the same intended use, different technological characteristics that do not raise additional questions of safety and effectiveness, and the information submitted to the FDA demonstrates that the devices are as safe and effective as the legally marketed device. The FDA lists several requirements for when a 510(k) is required. A 510(k) is required 90 days before attempting to sell the device, when there is a change or modification to a legally marketed device that could significantly impact the safety or effectiveness of the device, and when a legally marketed device is to be used for a different purpose. Class I and Class II devices are often exempt from 510(k) requirements because they do not pose the same safety risks. The FDA can decide whether a device is eligible for exempt status and not required to provide reasonable assurance of safety and effectiveness. A De Novo classification request is filed to classify novel medical devices when there is no predicate. A summary table produced by the FDA can be seen in Table 2.2.⁶²

Table 2.2. FDA classification of medical devices. Reproduced from ref (61).

Class	Risk	Potential Risk	Regulatory Controls	Submission Type or Exemption	Percent Devices in Class*
I	Lowest	Present minimal potential for harm	General	510(k) 510(k) Exempt *93% are exempt from 510(k)	35%
II	Moderate	Higher risk than Class I devices	General and Special (if available)	510(k) 510(k) Exempt	53%
III	Highest	Sustain or support life, are implanted, or present potential unreasonable risk of illness or injury.	General and PMA	PMA	9%

2.8.1. Proposed Device Classification

The expected classification for the device proposed in this work is a Class II medical device requiring 510(k)-approval. This is expected because audible sound is lower energy meaning that it should pose less risk to a patient when compared to ultrasound. This assessment is based on the FDA predicate seen in Table 2.3. outlining that a bone sonometer is most like the one proposed.⁶²

Table 2.3. FDA-predicated or equivalent bone sonometers reproduced from The US Food and Drug Administration. Reproduced from ref (59).

Device Name	Bone Sonometer
Regulation Description	“A bone sonometer is a device that transmits ultrasound energy into the human body to measure acoustic properties of bone that indicate overall bone health and fracture risk. The primary components of the device are a voltage generator, a transmitting transducer, a receiving transducer, and hardware and software for the reception and processing of the received ultrasonic signal. Reclassified from class 3 pma to class 2 510(k) 892.1180 [docket no. Fda-2005-n-0346] reclassification of bone sonometers”
Regulation Medical Specialty	Radiology
Review Panel	Radiology
Product Code	MUA
Premarket Review	Office of Radiological Health (OHT8) Division of Radiological Imaging and Radiation Therapy Devices (DHT8C)
Submission Type	510(k)
Regulation Number	892.1180
Device Class	Class II

The proposed device shares many of the same components such as the voltage generator, a transmitting transducer, receiving transducer, and hardware and software for the reception and processing of signals. The proposed device is different from the predicate because it introduces a secondary receiving transducer and lower frequency, audible sound waves. It is noteworthy that the 510(k) approval hinges on the idea that the FDA will find that audible sound poses less risk

than ultrasound and is as effective in providing information. If there is a question on substantial equivalence using ultrasound as the predicate, they may require a De Novo application.

2.9. Summary

The prevalence and risk associated with osteoporosis and other diseases that result in a reduction of BD drive the need for densitometric and sonometric devices. Although the markets associated with BD are large, there are concerns over the cost, availability, safety, and effectiveness of current densitometric and sonometric techniques. These concerns indicate a need for a new approach to monitoring BD. This is especially true in resource-constrained settings (i.e., global and rural health). Audible sound TDS represents a potential rapid, low-cost, and non-invasive approach to monitoring BD. If effective in monitoring changes in BD, the device shows potential as a commercialized product.

3. DEVICE DEVELOPMENT

3.1. Methods

3.1.1. Computational Method

The device uses TDS to measure the density and elastic modulus of a test sample. A cartoon of the device and the physical geometry of the measurement system is shown in Figure 3.1. The cartoon shows a transverse cross-section of the heel composed of the calcaneus and the surrounding soft tissue. The device uses a single speaker and two microphones that exist at distances d_1 and d_2 . Sound propagates from the speaker through a layer of soft tissue, bone, and a final layer of soft tissue before arriving at each microphone. This means that sound propagation time is a function of the material properties of the heel.

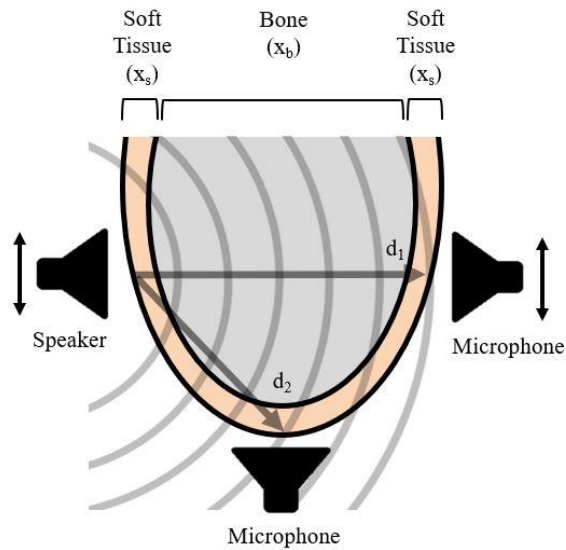


Figure 3.1. Cartoon of the device and physical geometry.

The velocity of a sound wave (v) can be written as a function of distance (d) and propagation time (t). The velocity of sound a sound wave propagating through a solid can also be written as a function of the material density (ρ) and elastic modulus (ε), thus relating the speed of sound to the material properties of the medium. Equation 3.1. shows this relationship. Based on Figure 3.1., the velocity of sound propagating through bone (v_b) can be written as a function of bone thickness (x_b), bone propagation time (t_b), soft tissue thickness (x_s), and soft tissue propagation time (t_s) shown in Equation 3.2. This approach assumes that the contribution from the surrounding soft tissue is negligible because it represents a small portion (13%) of the heel's composition.^{26,43,44} The computational governing equation is given by Equation 3.3. where propagation time through the bone is given as a function of bone thickness, elastic modulus, and density. Combining information from Figure 3.1. and Equation 3.3. bone thickness and propagation time can be measured while elastic modulus and density are unknown. This means that each microphone must be used to generate Equation 3.3. and used to solve a system of equations for elastic modulus and density.

$$v = \frac{d}{t} = \sqrt{\frac{\varepsilon}{\rho}} \quad (3.1.)$$

$$v_b = \frac{x_b}{t_b} = \frac{d-2x_s}{t-2t_s} \quad (3.2.)$$

$$t_b = \frac{x_b}{\sqrt{\varepsilon/\rho}} \quad (3.3.)$$

By applying TDS, the bone propagation time can be measured. Figure 3.2. shows an example of the expected electrical signals generated and acquired by the device in the geometry seen in Figure 3.1. At time equals zero, the sine wave at a given frequency is generated from the speaker. The first signal is acquired by the microphone that exists at distance d_2 and is shifted in time (Δt_1). The second signal is acquired by the microphone that exists at distance d_1 and is shifted in time (Δt_2). The shift in time (Δt) can be measured by a phase shift between the signals received by the microphones at d_1 and d_2 .

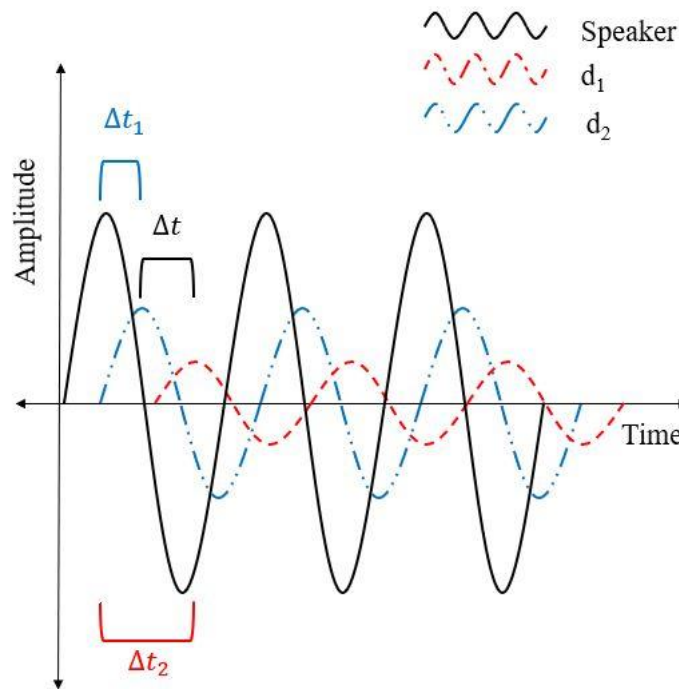


Figure 3.2. Example of the electrical signals used in TDS.

3.1.2. Deliverables

A device that can successfully apply TDS to assess bone health using audible sound must be able to accomplish three key tasks. The first task is that the device must be able to be quantitatively coupled to a test material to provide information on the contact between the device and the test material. The second task is that the device must be able to fit and measure the

geometries of the test material. The third task is that the device must be able to monitor the frequency and phase of the acoustic signal being transmitted through the test material.

3.2. Device Sensitivity

A sensitivity analysis was conducted to help understand the performance of the governing equation in describing the system. Sensitivity analysis is a tool used to understand the influence that independent variables (inputs) have on dependent variables (outputs).⁶³ This means that the results of sensitivity analysis can outline unrealistic model behavior and predict which parameters have the greatest impact on the system. There are two types of sensitivity functions, analytical and empirical. Analytical sensitivity functions are used to describe simple mathematical systems like the one used in this work. Empirical sensitivity functions are used for more complex, not well-mathematically defined systems. There are three primary types of analytical sensitivity functions, absolute, relative, and semi-relative. A relative sensitivity analysis was used in this work to compare the effects of different parameters (variables) on a system.

3.2.1. Relative Sensitivity Analysis

In a relative sensitivity analysis, a partial derivative of the governing equation is used to describe the slope around a normal operating point. Meaning that this approach shows how a percent change in an independent variable result in a percent change in the dependent variable. This relative sensitivity analysis assumes any contributions by the surrounding soft tissue are negligible because the soft tissue accounts for a small percentage of the human heel (~13%) and is less dense than bone. For this system, the normal operating points used in the calculation of each sensitivity function are given in Table 3.1. The normal operating points of a system are the expected values being reported for the system. The values in Table 3.1. are based on reported values of trabecular bone and ultrasound measurements.

Table 3.1. Normal operating points of the variables used in the governing equation. All values are based on that of trabecular bone and ultrasound wave propagation.

Variable	Range	Normal Operating Point (NOP)
¹⁶ Elastic Modulus (MPa)	10 - 3000	2200
^{16,64,65} Density (g/cm ³)	0.8 – 2.4	2.0
⁴⁴ Soft Tissue Thickness (mm)	-	8.4 ± 1.7
^{26,66,67} Speed of Sound (m/s)	1200 - 2100	1550
*Soft Tissue Transit Time (μs)	4 – 7	5
⁴³ Heel Thickness (mm)	50 – 80	65

*Calculated based on the speed of sound and soft tissue thickness.

Given the governing equation has three independent variables, this means that three relative sensitivity functions must be used to determine how sensitive the governing equation is to changes in each variable. In other words, the three sensitivity equations provide clarity on how sensitive the propagation time measurement is to changes in density, thickness, and elastic modulus of bone. The equations are shown in Equations 3.4., 3.5., and 3.6., where t_b is the propagation time of sound through bone, x_b is the thickness of bone, ϵ is the elastic modulus of bone, and ρ is the density of bone. Equation 3.4. is the bone density sensitivity function. Equation 3.5. is the bone thickness sensitivity function. Equation 3.6. is the elastic modulus sensitivity function.

$$\bar{S}_{\rho}^{t_b} = \frac{x_b}{2(\epsilon^{0.5})(\rho^{0.5})} * \frac{\rho}{t_b} |_{NOP} \quad (3.4.)$$

$$\bar{S}_{x_b}^{t_b} = (\rho/\epsilon)^{0.5} * \frac{x_b}{t_b} |_{NOP} \quad (3.5.)$$

$$\bar{S}_{\epsilon}^{t_b} = \frac{-x_b(\rho^{0.5})}{2(\epsilon^{1.5})} * \frac{\epsilon}{t_b} |_{NOP} \quad (3.6.)$$

The relative sensitivity calculation was completed in MATLAB R2020A, and the results are shown in Figure 3.3. In Figure 3.3., the density, elastic modulus, and bone thickness functions are stable across the expected range of heel thicknesses. This means that for both thick and thin feet, the propagation time sensitivity remains relatively constant. The magnitude of each of the functions shows that the propagation time sensitivity is the most sensitive to changes in density. This is ideal for a testing system that is focused on calculating the density of bone based on propagation time.

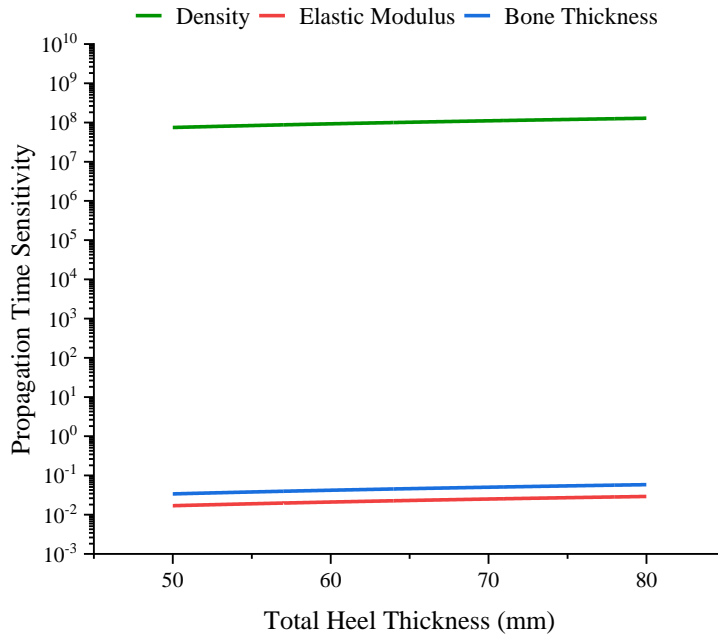


Figure 3.3. Graph of the log scale propagation time sensitivity across the range of expected heel thickness.

3.2.2. Microphone Position Sensitivity

A similar sensitivity calculation was performed to inform the decision of where the microphones should be positioned relative to each other on the heel. For this sensitivity analysis, three microphone positions were imagined and are shown in Figure 3.4. In the first scenario,

distance d_1 is greater than distance d_2 . In the second scenario, distance d_1 is equal to distance d_2 . In the third scenario, distance d_1 is less than d_2 .

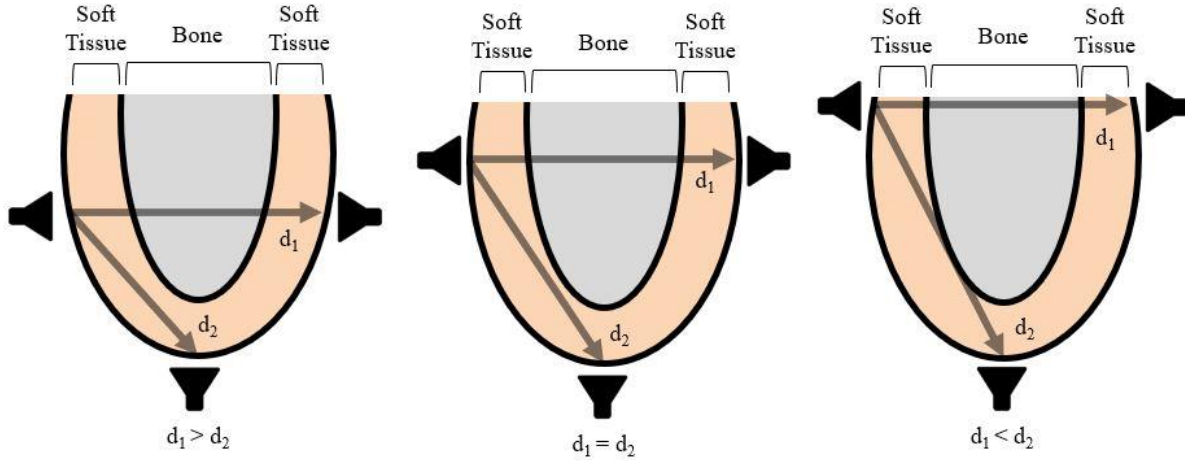


Figure 3.4. Microphone positioning scenarios used for the microphone positioning sensitivity analysis.

The governing equation for this sensitivity analysis is given by Equation 3.7. where Δt is the change in propagation time, x_{b1} is the thickness of bone across distance d_1 , x_{b2} is the thickness of bone across distance d_2 , ρ is the density of bone, and ϵ is the elastic modulus of bone. This equation was derived by taking the difference between the propagation times for each path length.

$$\Delta t = \frac{x_{b1}}{(\epsilon/\rho)^{0.5}} - \frac{x_{b2}}{(\epsilon/\rho)^{0.5}} \quad (3.7.)$$

Based on Equation 3.7., the resulting microphone position sensitivity to changes in density is shown by Equation 3.8. Only a density sensitivity function was derived for this analysis because the system is the most sensitive to changes in density.

$$\bar{S}_{\rho}^{\Delta t} = \frac{0.5x_{b1} - 0.5x_{b2}}{(\epsilon^{0.5})(\rho^{0.5})} * \frac{\rho}{t_b} |_{NOP} \quad (3.8.)$$

The results are shown in Figure 3.5. This plot outlines that the system is the most sensitive to a difference in propagation time between the two microphones when the distances are different.

This is evident by the larger Δt sensitivity seen at the minimum and maximum Δ Distance bounds. This means that the physical device should aim to make the path lengths different to improve the ability to determine a difference between propagation times along both paths.

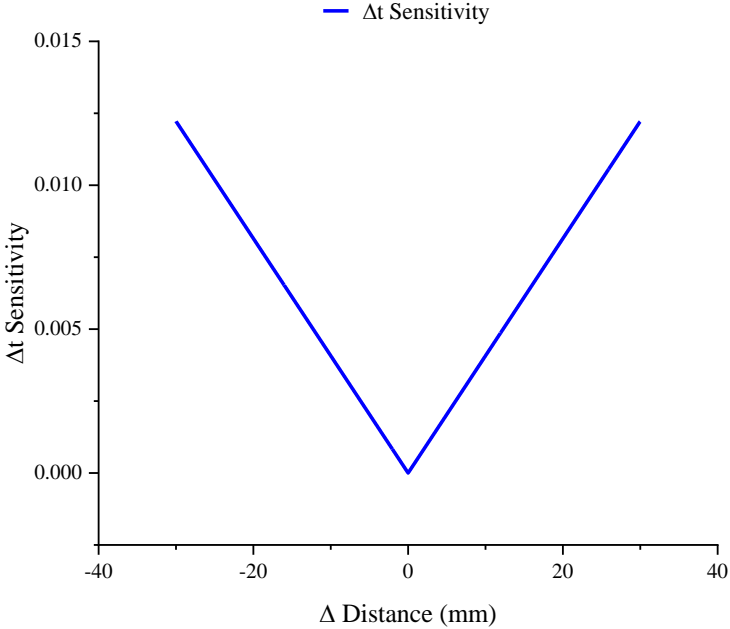


Figure 3.5. Graph of the difference between microphone distances (d_1-d_2) versus the difference in propagation time sensitivity.

3.3. Device Hardware

3.3.1. Alpha (α) Prototype

The α -prototype was the first prototype constructed for this work and is pictured in Figure 3.6. The device used a single speaker (Aftershokz Sportz 3 Bone Conduction Headphones) and two microphones (Edutige EIM-001 Omnidirectional 3.5 mm, 4-pole microphone) to generate and acquire audio data, respectively. The speaker was connected to a laptop using the 3.5mm audio jack and the microphones were each connected to a USB port. The basic mechanics of the device were based on a pressure plate and fixation arms. As the patient places their foot on the pressure plate, the fixation arms clamp around their foot. After clamping on the medial and lateral sides of the foot, the length adjustment housing can be tightened securing the foot in place. The toe alignment structures were added as an additional method of keeping the foot in place. Although the device was simple to use, the prototype was succeeded by the β -prototype because it could not readily measure the coupling force of the device, the distance between the speaker and microphones, and control the signals being generated.

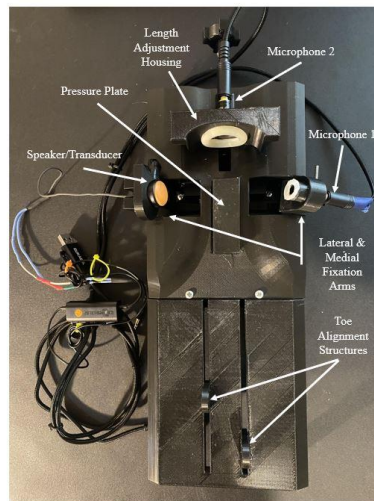


Figure 3.6. Picture of the α -prototype.

The inability to generate sinusoidal, acoustic signals was a main reason for moving away from the α -prototype. This became apparent through the validation of LabVIEW's ability to generate sound. In the experiment, LabVIEW was used to generate a sine wave of a given frequency. The generated signal was then measured across the positive and negative terminals of the speaker. The α -prototype used an Aftershockz Sportz 3 bone conduction headphone and the β -prototype used a CMS-28588N-L152 speaker. Figure 3.7. describes the method and shows an example of a 10 kHz LabVIEW-generated signal along with the corresponding measurements from the α and β -prototype speaker. The measured wave from the α -prototype appears most like a square wave which is noticeably different from the LabVIEW-generated sine wave. This is likely an artifact of the power and volume unit connected to the α -prototype speaker. The measured wave of the β -prototype appears most like a sine wave which matches the LabVIEW-generated sine wave.

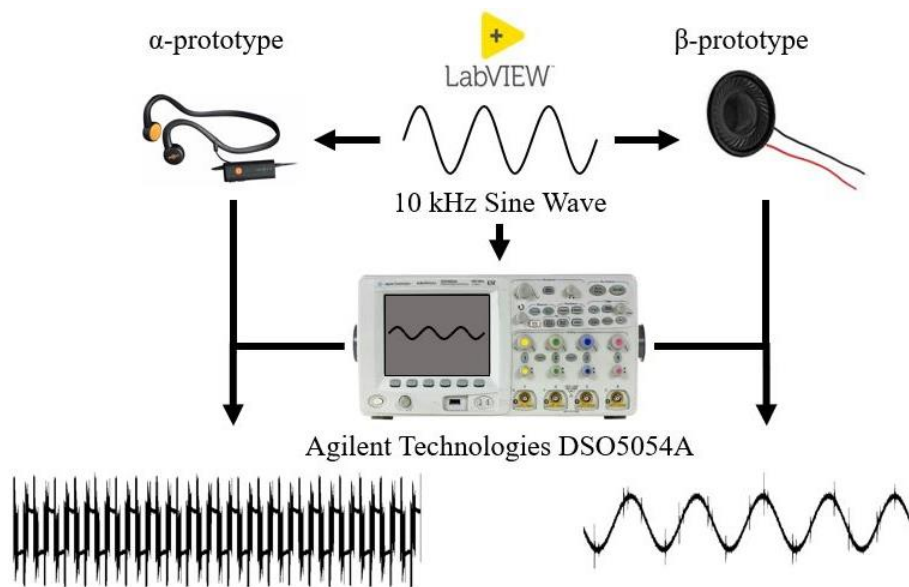


Figure 3.7. Description of the electronic signals test done using the speaker from the α and β -prototypes.

3.3.2. Test Bed - Beta (β) Prototype

To assess the feasibility of the methods and satisfy the deliverables of the project, a test bed was constructed. A picture of the test bed is shown in Figure 3.8. This device shares several of the same characteristics as the α -prototype. For example, the device uses a speaker and two microphones to generate and record audio data. The device differs from the α -prototype in the type of microphone and speaker used and through the addition of the linear actuators, 4 channel relays, current sensors, and control boards.

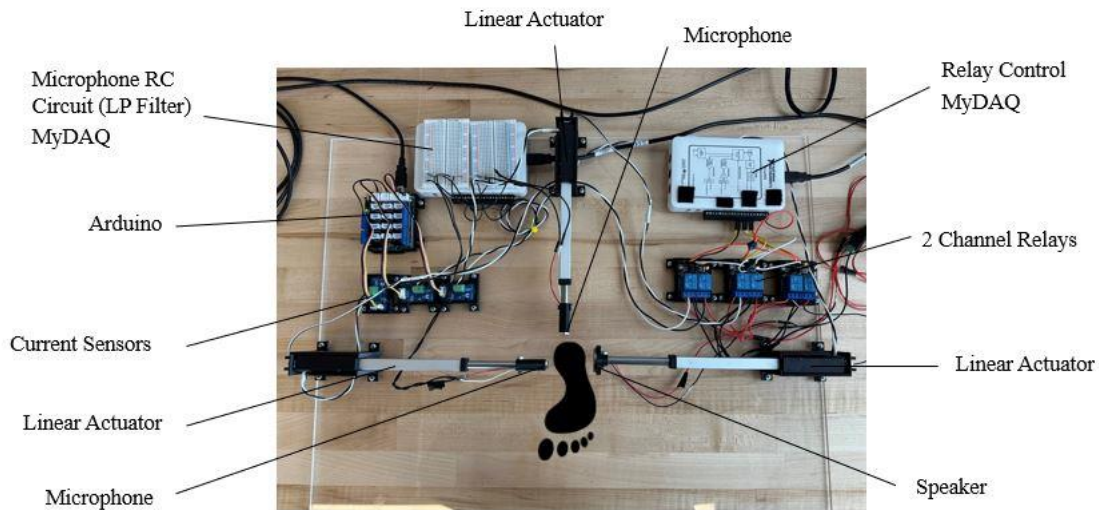


Figure 3.8. Picture of the β -prototype test bed.

The microphone used in the β -prototype is a CMA-454PF-W electret condenser microphone. It was selected over dynamic, ribbon, and traditional condenser microphones because they are small, affordable, do not require an external power supply, and are sensitive to the audible frequency range.⁶⁸⁻⁷¹ Figure 3.9. shows a wiring diagram and the microphone measurement circuit used in the device. The microphone measurement circuit features a DC Blocking, Lowpass filter with an $8\text{k}\Omega$ resistor and 1 nF capacitor for a cutoff frequency of 19.9 kHz . The microphone circuits were connected to an NI MyDAQ device in a differential analog configuration. The microphone 180° from the speaker was connected to the analog $0+$ and $0-$ channels while the 90° microphone was connected to the analog $1+$ and $1-$. A wiring diagram of the microphone circuit integrated with the MyDAQ is shown in Figure 3.9. The speaker used in the β -prototype was a CMS-28588N-L152 speaker that was selected because it was affordable and could generate the audible sound spectrum. The speaker was wired to a 3.5 mm audio jack and plugged directly into a computer. The combination of the speaker and microphones enables signal generation and acquisition, respectively.

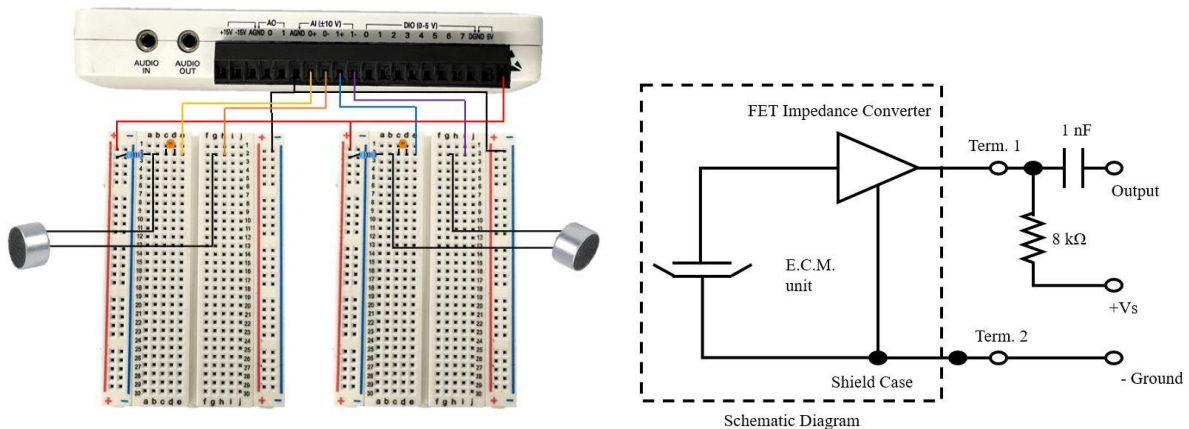


Figure 3.9. Wiring diagram of the microphone system (left) and microphone measurement circuit (right).

The linear actuators used in the device are continuous 4" PA-07 Series DC Micro Linear Actuators from Progressive Automations. Although a stepper motor might have been a better selection for the device because of their applications in position control, continuous DC motors were selected because the initial intended use of the actuators was simply to hold the foot in place. However, the continuous DC motors can be used within a feedback response system and calibrated for position based on a software timing system. For this device, the feedback loop is based on the current load on the motor; as the load (force) at the end of the actuator increases, the current drawn by the motor will increase. The continuous motors can also be easily controlled using 2 channel relays connected to an NI MyDAQ and LabVIEW Boolean logic. The relays are used to control when the actuator gets power from the external 12V 5A power supply and the direction of rotation which dictates whether the actuator extends or retracts. A wiring diagram of the actuators, relays, and power supply is shown in Figure 3.10.

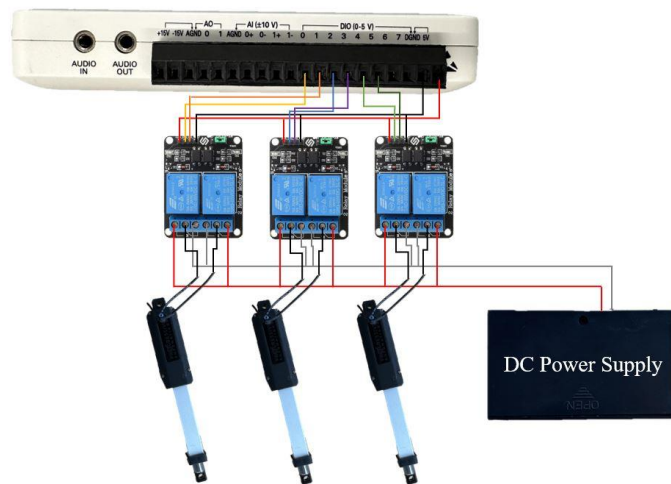


Figure 3.10. A wiring diagram of the system that controls the linear actuator movement.

The current load on the linear actuator motor will be monitored by an ACS70331 Grove 2.5A - DC Current Sensor. This sensor was selected because it has a 0 – 2.5-amp (A) sensing range

with an 800 mV/A typical sensitivity. This works well with the linear actuator which has a current range from 0.1 A to 0.2 A. Each actuator has a corresponding current sensor that is connected to an Arduino Uno R3. The Arduino is connected to a laptop and easily interfaced with LabVIEW. A complete wiring diagram of the current sensor, Arduino, and the linear actuators is shown in Figure 3.11.

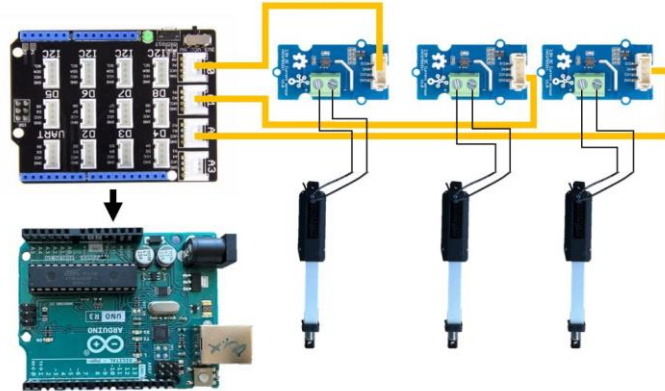


Figure 3.11. A wiring diagram of the system that monitors the current drawn by the linear actuators.

3.3.3. Cost

A complete list of the hardware components used in this work is shown in Table 3.2. The components have been categorized based on the prototype. The total cost to construct the α and β -prototype was \$173.65 and \$755.82, respectively. For reference, the low-end cost of a used QUS device can be estimated at \$2,0000. This means that there is a 91.3% and 62.2% reduction in price between used QUS devices and the α and β -prototype, respectively. For the future commercially available device, the expected cost reduction will likely fall between those estimated for the alpha and beta prototypes. This is because significant cost reduction of the final device can be achieved by eliminating one or both NI myDAQs with a custom printed circuit board.

Table 3.2. Hardware materials list for the alpha (α) and beta (β) prototype.

Quantity	Component Description – Model Information	Prototype	Cost per unit (\$)
2	Edutige Microphone – i-Microphone EIM-001 Omnidirectional 3.5 mm 4-pole (TRRS)	α	27
1	Aftershokz Bone Conduction Headphones – Sportz 3	α	100
624 g	Polylactic Acid – HATCHBOX 1.75mm Black PLA 3D Printer Filament	α	0.024
8	Washers – #6 Everbilt Zinc, Flat Washers	α	0.0689
10	Self-Drilling Screws – #6 1/2” Screws	α	0.0346
1	Spring – 1/2" Compression Spring	α	\$3.78
Total Cost of the α – prototype			173.65
2	Electret Condenser Microphones – CMA-4544PF-W	β	0.665
1	Speaker – CMS-28588N-L152	β	3.97
137 g	Polylactic Acid – HATCHBOX 1.75mm Black PLA 3D Printer Filament	β	0.024
1	Plexi Glass – 36” x 48” x 0.093” Clear Acrylic Sheet	β	57.38
2	National Instruments MyDAQ	β	199.95
1	Arduino Uno R3	β	28.50
1	Grove Base Shield V2.0 for Arduino	β	3.50
3	Current Sensor – Grove 2.5A - DC Current Sensor - ACS70331	β	8.70
3	Mechanical Relays – 2 Channel 5V Relay Module	β	6.76
3	Linear Actuators - 4” PA-07 Series Micro Linear Actuator from Progressive Automations	β	70
40	Self-Drilling Screws – #6 1/2” Screws	β	0.0346 per screw
The total cost of the β -prototype			755.82

3.4. LabVIEW Virtual Instruments (VI)

LabVIEW virtual instruments (VI's) were used in this project as the primary software package. LabVIEW is a graphical programming language and was selected because it is commonly used as a development package where controlling, data acquisition, and computations required for an instrument can be completed. For the β -prototype, LabVIEW was used to generate the audio signal, acquire the audio signal, control the motion of the linear actuators, and integrated with Arduino to measure the current drawn by the actuators.

The audio signal was generated using a LabVIEW SV Signal (Waveform) function. An SV Configure Generator function was used to define the amplitude, frequency, duration, and profile of the generated waveform. The Configure Generator function was used because it can be configured to support different waveform types (sine, square, triangle) and it can be used to sweep frequencies in a linear or logarithmic manner. The configured and generated signal is then sent to the speaker using the Play Waveform function. A complete diagram of the sound generation VI is shown in Figure 3.12.

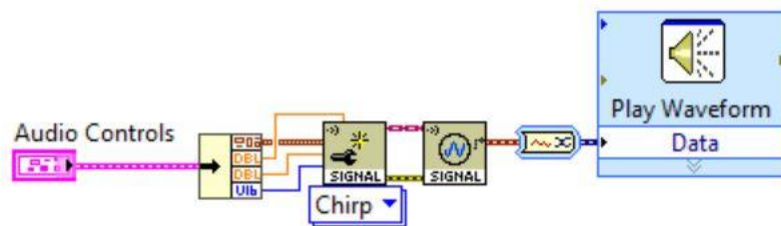


Figure 3.12. LabVIEW block diagram representation of the functions used to generate the audio signal.

The audio signal was recorded using a LabVIEW DAQ Assistant function. With this function, audio data from the microphones can be recorded continuously by controlling the acquisition device, the sampling rate, and the number of samples. The DAQ Assistant was selected because it could easily be configured for continuous data acquisition. The DAQ Assistant could also be configured to complete discrete measurements. A complete diagram of the sound acquisition VI is shown in Figure 3.13.

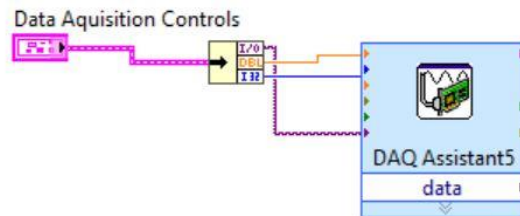


Figure 3.13. LabVIEW block diagram representation of the functions used to acquire the audio signal.

The motion of the linear actuators was controlled using a LabVIEW DAQ Assistant Function. With this function, 2-channel relays could be controlled using the digital output lines on the MyDAQ. They allowed LabVIEW to regulate the power given to the actuators and their extension or retraction. A series of nested case structures and while loops were used to select which actuator is being controlled and whether it is extending, retracting, or stationary. The control of the actuators was integrated with a serial reading of the data from current sensors through the Arduino. The Arduino readings are then put into LabVIEW to control when the actuators stop their extension. An example diagram of the force-integrated feedback loop and actuator control is shown in Figure 3.14.

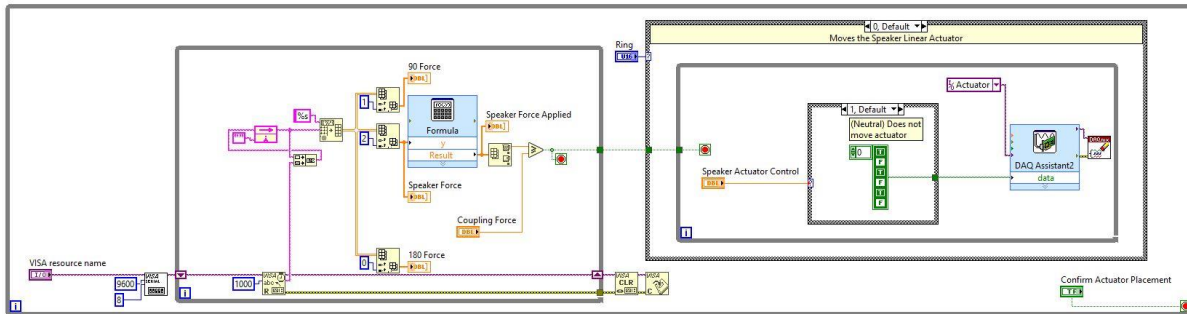


Figure 3.14. LabVIEW block diagram representation of an example script that monitors the current given to the actuator, the corresponding force, and stops the motion of the actuator based on the force reading.

3.5. Device Resolution

The resolution of a measurement system is the smallest unit that differentiates two values that are approximately equal.⁷² For the final device to be effective, the resolution of the BD measurement must be able to detect clinically relevant changes in BD. The determination of the BD resolution is based on the resolution of the sound propagation distances and time delay between signals. The estimated distance resolution of the device is 0.01 inches. The resolution of the time delay is based on the specifications of the NI MyDAQ. The MyDAQ features a 16-bit analog-to-digital converter (ADC) with a maximum sampling rate of 200 kS/s. With a bit depth of 16 and a 10-volt (V) measurement range (i.e., -5 V to 5 V), the voltage resolution of the device is 15.3 μ V. The time resolution of the system reported by NI is 10 ns. At 20 Hz and 20 kHz a 10 ns time resolution is equal to a $7.2E-5^\circ$ and 0.072° phase shift, respectively. The sampling rate of 200 kS/s is suitable for this application because the maximum frequency to be measured is 20 kHz. This means the device can sample well beyond the Nyquist Limit of twice the frequency at ten times the measured frequency. Sampling at ten times the maximum frequency ensures that the waveforms will be adequately sampled and be able to resolve the amplitude, frequency, and phase.

3.6. Device Safety

Although an extensive safety and risk assessment for this device will likely be required in the future, a preliminary safety assessment has been completed. The study was focused on the safety of patients and providers for a device that uses audible sound. According to the office of Occupational Safety and Health Administration (OSHA), hearing conservation measures are required when noise exposure is at or above 85 decibels (dB) average for over eight working hours. To test this, a decibel meter application on an iPhone was used. The iPhone microphone was placed in contact with the β -prototype speaker representing an extreme scenario of device use (equivalent to a provider or patient putting their ear against the speaker). At different computer volumes, a frequency sweep across the upper end of audible spectrum was completed with the sound amplitude being recorded. The results are given by Figure 3.15.

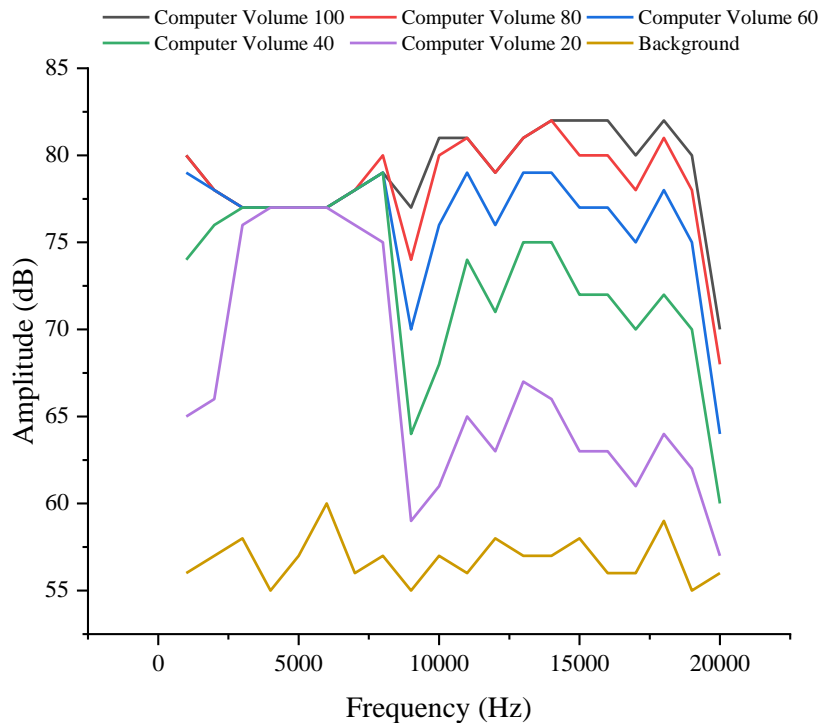


Figure 3.15. Amplitude of the device in decibels across the upper end of the audible frequency spectrum outlining the device safety.

The device passed this OSHA safety requirement because it did not exceed 85 dB. For reference, the sound level of the device is comparable to a vacuum cleaner (~ 70 dB) or a blender (~ 80 dB) and should not be used for more than a couple minutes for the test. These preliminary findings show that the device is safe to continue research.

4. EXPERIMENTS

4.1. Frequency and Phase Experiment

4.1.1. Introduction

Before testing the device prototype on bone or bone phantoms, the ability of the NI MyDAQ to measure frequency and phase was assessed. The experiments were focused on assessing the variability of the device in measuring frequency and phase across the audible frequency range. The frequency and phase of a signal are important because the time delay between the signals is dependent upon their individual frequency and phase. A fast Fourier transform (FFT) approach was used to calculate the frequency and phase of each signal. Effective measurements of frequency and phase mean that the MyDAQ, LabVIEW, and the FFT-based computational approach can measure the primary features of a given signal.

4.1.2. Methods

In the experiment, simulated microphone signals were generated using a Tektronix AFG3252C arbitrary function generator. The function generator has two output ports and can regulate the frequency and phase of each signal. Output ports 1 and 2 from the function generator were connected to the microphone input ports on the MyDAQ. This means that if the signals from the 90° and 180° microphones were pure sine waves, the MyDAQ, and software can measure the frequency and phase of the generated wave, thus confirming its effectiveness within this application. The electrical signals were acquired and analyzed using LabVIEW 2019.

The frequencies used within the experiment were selected based on the audible sound spectrum and range from 1 kHz to 20 kHz. The frequencies were selected because they represent the higher end of the audible sound spectrum. The phases used in the experiment were 0°, 45°, 90°, and 180°. The phase shifts were selected based on sample calculations of expected ultrasonic phase shifts. The values used for the speed of sound propagation and heel thickness are found in Table 3.1. which outlines the normal operating points of the system. Figure 4.1. shows the results of the expected phase calculation. The plot on the left shows that for the range of audible frequencies, differences in path lengths between the microphones based on heel geometries, and speeds of recorded ultrasound propagation the range of expected phase shift values are from 0° to 180°. The plot on the right shows the logarithmic representation of the expected phase shift to outline the differences between sound propagation at 1200 m/s versus sound propagation at 2100 m/s. Combining the information from both plots establishes the test parameters for the phase experiment.

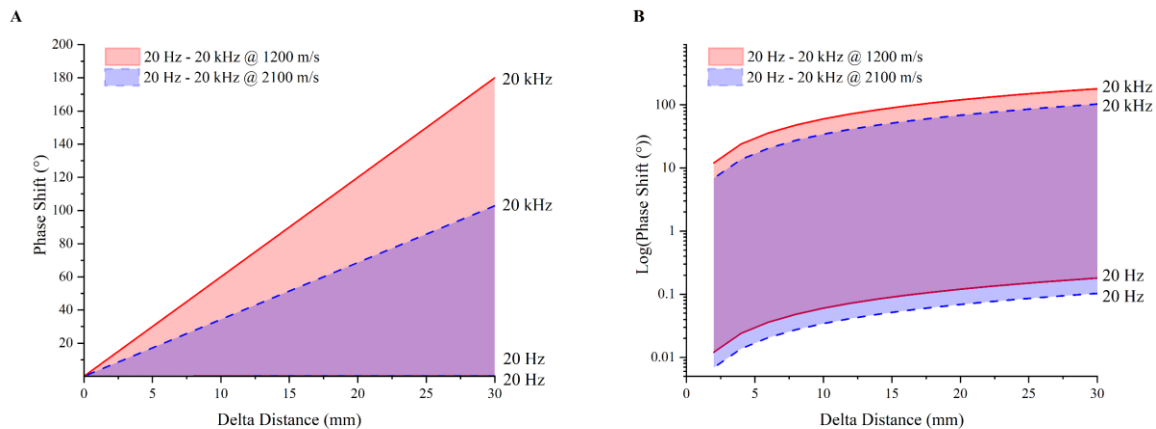


Figure 4.1. Plots of the expected phase shift of the system.

The acquisition and subsequent computations to calculate the frequency and phase of the waves were completed in the same LabVIEW VI's. The block diagram VI is shown in Figure 4.2. In this VI, an NI DAQ Assistant is used to acquire the voltage readings from the differential analog

input (AI) ports zero (AI 0 \pm) and one (AI 1 \pm). The VI computes the corresponding frequency and phase of the two individual waveforms using the Tone Measurement function that makes use of an FFT. The phase shift between the two signals is then calculated based on the difference between the individual phases of the wave. The amplitude, frequency, phase, and phase differences of the two waves are then written in a measurement file. This process can be repeated by adjusting the number of iterations of the for loop that contains the acquisition functions.

The sampling frequency and number of points used in the experiment were constant at 200 kHz and 1000 points, respectively. The for loop was set to 100 iterations meaning that it would sample the wave, calculating the frequency, phase, and phase difference, 100 different times before terminating the data acquisition. These 100 data points were then written to a data file with the name of the file containing their expected frequency and phase shift designation.

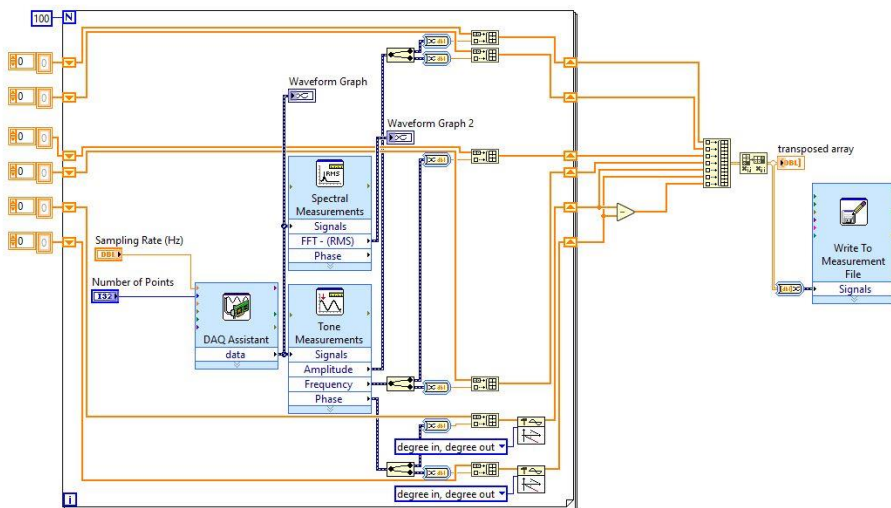


Figure 4.2. LabVIEW block diagram representation of the VI used to acquire signal and compute the frequency and phase.

The performance of the NI-MyDAQ's ability to measure the frequency and phase of a signal was assessed using a relative root mean square error (RRMSE). The RRMSE is used to quantify the relationship between the expected frequency and phase versus the measured frequency

and phase, respectively. The RRMSE calculation is shown in Equation 4.1. where y_i is the expected frequency or phase value and \hat{y}_i is the measured frequency or phase value.

$$RRMSE (\%) = \sqrt{\frac{\frac{1}{n} \sum_{i=1}^n (y_i - \hat{y}_i)^2}{\sum_{i=1}^n (\hat{y}_i)^2}} * 100 \quad (4.1.)$$

The variance of the frequency (σ_f/f) and phase (σ_p/f) normalized by frequency was used as an analog to a 1/f noise measurement. A 1/f noise measurement is useful in assessing the variability of a measurement system and is expected to decrease as frequency increases.

4.1.3. Results

The results of the expected frequency experiment are shown in Figure 4.3. where the expected frequency is plotted against the frequency measured by the MyDAQ. The RRMSE (%) for the fit of signals one and two to that of the expected values were 0.301 % and 0.302 %, respectively.

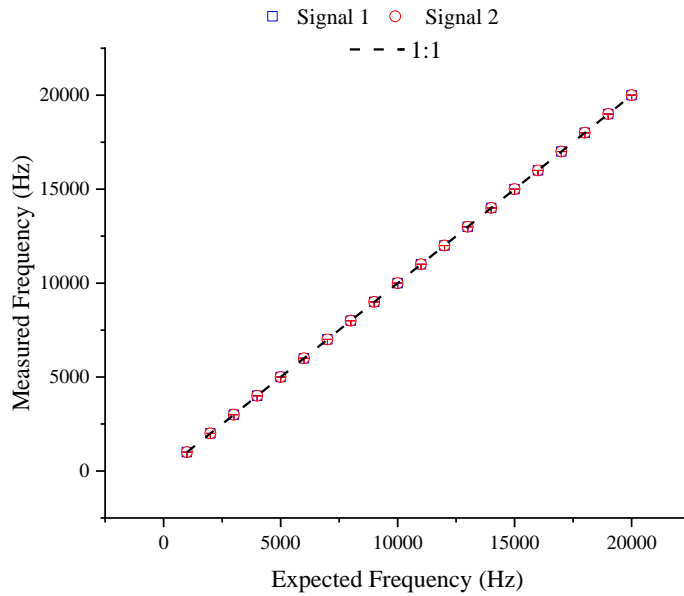


Figure 4.3. Q-Q plot of the expected frequency versus the measured frequency.

The results of the expected phase experiment are shown in Figure 4.4. where the expected phase shift and the measured phase shift are plotted across the range of frequencies tested. The RRMSE (%) for the fit of the expected phase to the measured phase was 53.6 %, 53.6 %, 53.6 %, and 53.6 % for the 0°, 45°, 90°, and 180° phase shift, respectively. The RRMSE (%) was calculated based on the difference between the measured phase and the expected phase which is shown in Figure 4.4. The systematic error for each phase series ranged from 0.897° at 1 kHz to 17.9° at 20 kHz.

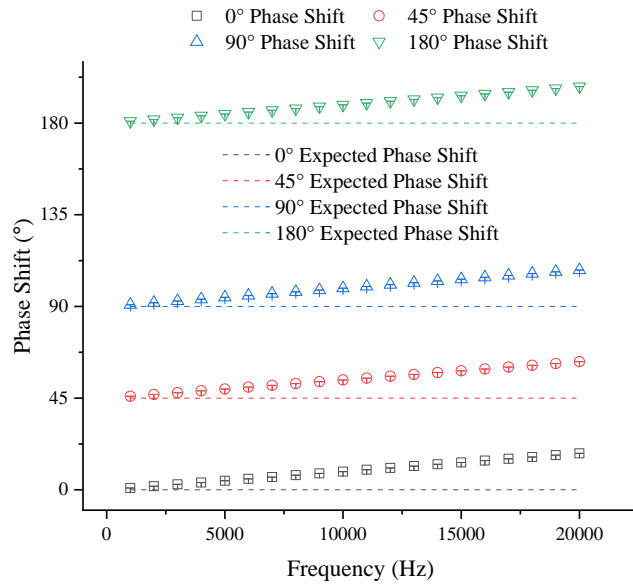


Figure 4.4. Measured phase shift between two signals across the phase and frequency range.

The σ_f/f and σ_p/f values across the frequencies of interest are shown in Figure 4.5. and Figure 4.6., respectively.

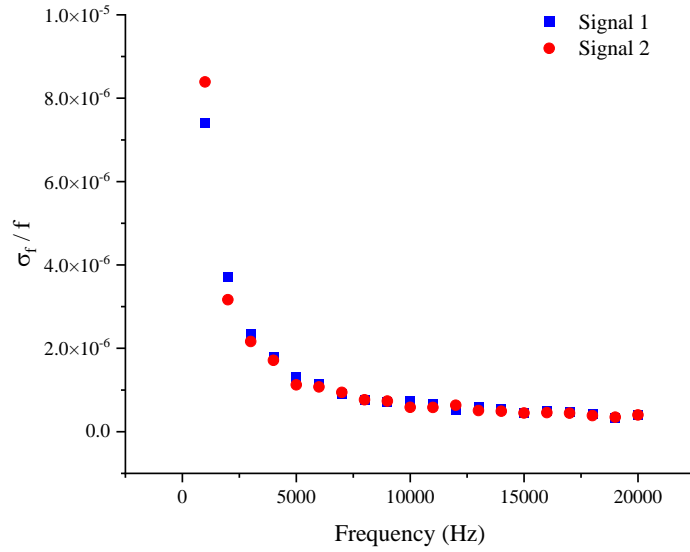


Figure 4.5. σ_f/f across the frequency range of interest.

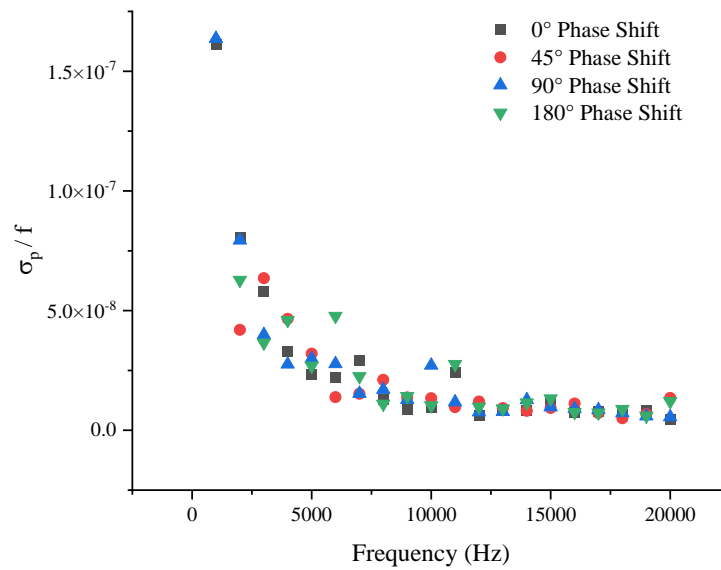


Figure 4.6. σ_p/f across the frequency range of interest.

4.1.4. Discussion

The results of the frequency experiment show that the MyDAQ and the constructed LabVIEW VI can effectively measure the frequency of a wave. This is shown by the low RRMSE (%) of 0.301 % and 0.302 % of the two signals measured in the experiment. These values are much less than 10%, indicating an excellent fit and high accuracy between the expected frequency and the measured frequency.⁷³ The variance normalized by frequency (σ_f/f) is low relative to the frequency of the wave outlining low variability and indicating a precise measurement. The combination of the RRMSE (%) and the σ_f/f support the initial hypothesis that the MyDAQ, LabVIEW VI, and the FFT-based computational approach can effectively measure the frequency of a signal.

The results of the phase experiment show that the MyDAQ, LabVIEW VI, and FFT-based computational approach display a systematic error. The systematic error is evident in Figure 4.7.

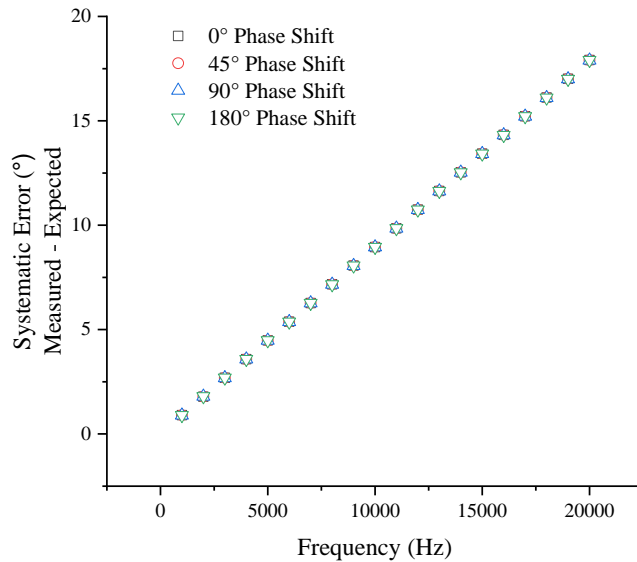


Figure 4.7. Phase variance between the measured and expected phase shift across the frequency range.

where the difference between the measured and expected phase increases as frequency increases. The systematic error between the expected and measured phase shift is linear and ranges from 0.897° at 1 kHz to 17.9° at 20 kHz which is equivalent to a $2 \mu\text{s}$ time delay. This systematic error is reflected in the RRMSE (%) fit of 53.6 % for the 0° , 45° , 90° , and 180° phase shifts. The phase shift is likely due to the combination of the multiplexer and ADC converter in the MyDAQ. This error corresponds to a constant time delay. The linear nature of the systematic error means that calibration can be completed using the linear trend seen in Figure 4.7.

The results of the calibrated phase difference plot are shown in Figure 4.8. where the values have been adjusted by the systematic error at a given frequency. The plot shows that the phase shift closely follows the expected phase shift. This observation is supported by the low RRMSE (%) of 0.019 %, 0.015 %, 0.017 %, and 0.018 % for the 0° , 45° , 90° , and 180° phase shift, respectively. Each of those values is much less than 10%, indicating an excellent fit.⁷³ The average

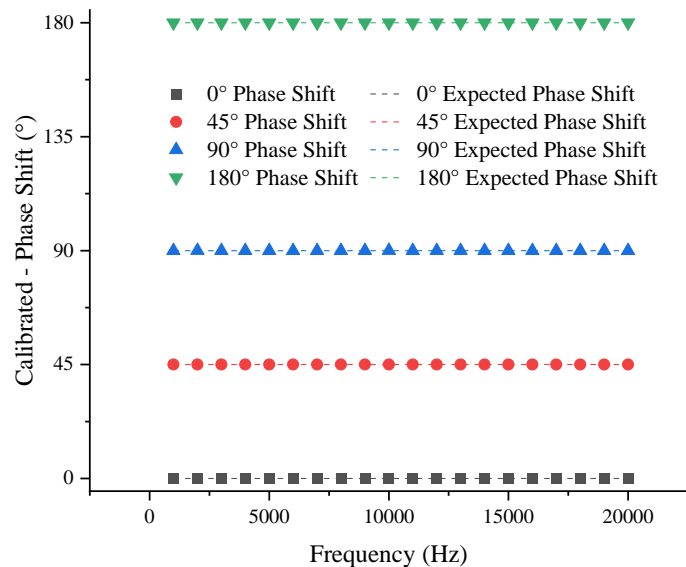


Figure 4.8. Calibrated measured phase shift between two signals across the phase and frequency range.

standard error across the calibrated phase series and frequencies was 0.003° . The combination of the RRMSE (%) and the average standard error supports the initial hypothesis that the MyDAQ, LabVIEW VI, and the FFT-based computational approach can measure the phase of a signal after calibration.

When taking the frequency and phase of a signal, special consideration should be paid to the power supply that is used in the device. The device initially used an Alitov ADC (Model Number: ALT-1205) as a power supply for the linear actuators. Preliminary testing of the device showed an injection of high frequency noise that is commonly associated with ADC. Figure 4.9. illustrates the injection of high frequency noise with the signals being 7.5 kHz sine waves sampled at 200 kHz with 1000 points. Signals 1 and 2 (ADC) represent signals measured with the ADC power conversion connected to the system while signal 1 and 2 represent signal measured without the ADC connected to the device. The striking difference between the signals with and without the

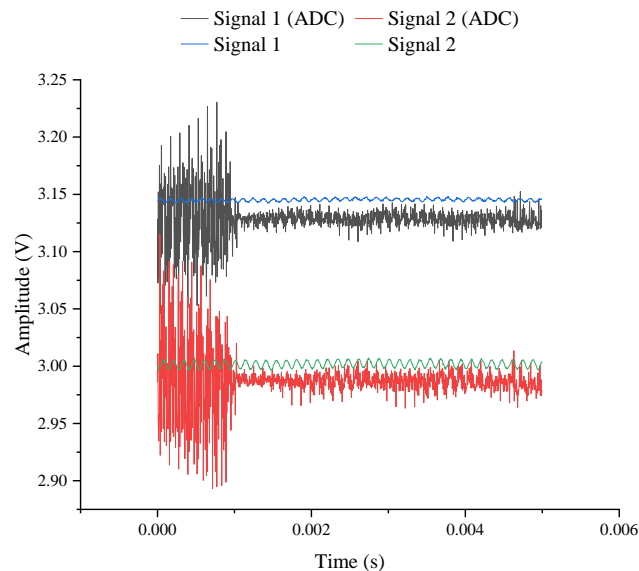


Figure 4.9. Injection of high frequency noise from the power supply ADC.

ADC connected means that the device must either find a higher quality ADC that does not inject the same quantity of high frequency noise, find a rechargeable DC power supply, or separate the actuator power and control from the measurement circuits. Using a higher quality ADC or a rechargeable DC power supply may increase the cost of the device significantly, but they appear to be better options than separating the measurement circuit from the actuators because they are joined at the laptop that runs the device.

4.1.5. Conclusions

The frequency and phase experiment confirmed the ability of the MyDAQ, LabVIEW, and FFT-based methods to measure the frequency and phase of two simulated microphone signals. A low RRMSE and σ_f/f show the frequency measurement is accurate and precise. The phase experiment required calibration to correct for the linear, systematic error observed in the experiment. The calibration was able to successfully correct the systematic error, resulting in a low RRMSE and σ_f/f showing the phase measurement is accurate and precise. The injection of high frequency noise by the device power supply should be closely monitored in the device moving forward.

4.2. Actuator Coupling Force & Speed

4.2.1. Introduction

Ultrasonic methods of measuring bone density use ultrasound coupling gels to ensure good contact between the transducers and the body. This means that in any acoustic measurement system, the quantification of coupling force must be recorded. For the proposed audible measurement system, the coupling force measurement is based on the relationship between direct current (DC) and applied load at the end of a linear actuator. The relationship between current and applied actuator force is direct meaning that as the applied force increases, the current supplying

the actuator increases. The purpose of the experiment is to generate calibration curves for each actuator used to monitor the coupling force between the system transducers and the body.

4.2.2. Methods

To measure the relationship between current and applied force a linear actuator, current sensor, and Arduino were used. The linear actuator used was a 4" PA-07 Series Micro Linear Actuator from Progressive Automations. The current sensor used was a Grove 2.5A DC Hall Effect Current Sensor ACS70. The Arduino used was an Arduino Uno R3. The methods flow diagram is shown in Figure 4.10. and represents the testing protocol used. The test begins with the linear actuator moving a known calibration weight. As the actuator moves the weight, the current sensor measures the voltage and relates it to the current using Equation 4.2. where current (I) is written as a function of voltage (v), offset voltage (v_{offset}), and the current sensor sensitivity (I_s ; 800 mV/1000 mA). The Arduino computes the current and writes the data to LabVIEW where it is recorded and displayed.

$$I = (v - v_{offset})(I_s) \quad (4.2.)$$

A flow diagram and image of the test setup are shown in Figure 4.10. First, the actuator was extended under a known physical load. During extension, readings of the current load on the DC motor were taken using the current sensor and Arduino. The LabVIEW program then collected the current readings and recorded the maximum current value. The time of full extension under a physical load was also recorded to understand how the actuators move under load. From the recorded data, calibration curves for each of the three actuators were generated plotting load versus current and load versus speed. A weighted linear fit from Origin was used to create the calibration curves. The plots of speed versus load and current versus load were then compared with the linear actuator specifications given in Table 4.1.

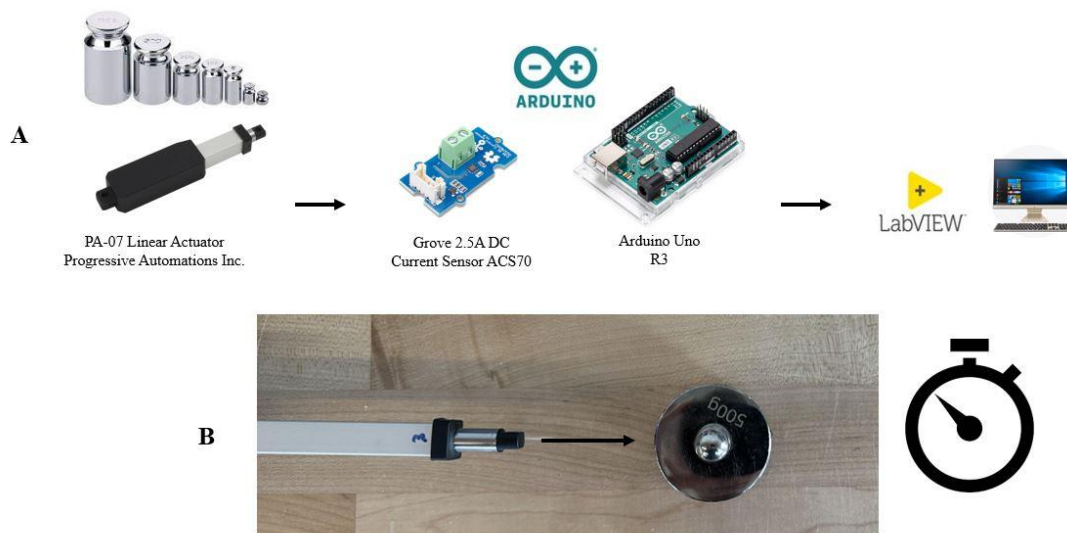


Figure 4.10. Method flow diagram of the microphone and speaker coupling force experiment (A) and picture of the test setup (B).

Table 4.1. Specifications for a 4” PA-07 Series Micro Linear Actuator from Progressive Automations.

Dynamic Load (kg)	Static Load (kg)	No Load Current (mA)	Full Load Current (mA)	No Load Speed (in/s)	Full Load Speed (in/s)
2.27	2.95	100	200	0.59	0.55

4.2.3. Results

The results from the load and current calibrations are shown in Table 4.2. and Figure 4.11. Table 4.2. displays the values and standard error for the intercepts and slopes for linear calibration equations in addition to the adjusted R-Square value. For the speaker actuator, the intercept was 82.2 ± 1.86 with a slope of 0.008 ± 0.002 . For the 90° Actuator, the intercept was 96.4 ± 1.01 with a slope of $0.006 \pm 7.29E-4$. For the 180° Actuator, the intercept was 97.1 ± 0.349 with a slope of $0.005 \pm 3.21E-4$. The adjusted R-square values for speaker, 90° , and 180° actuators were 0.814, 0.926, and 0.976, respectively. The slopes of the load versus current calibration curves were significantly different than zero at the 95% confidence interval.

Table 4.2. The intercept, slope, standard error (SE), and the adjusted R-square value for the load versus current calibration data.

	Intercept		Slope		Adj. R-Square
	Value	SE	Value	SE	
1. Speaker Actuator	82.2	1.86	0.008	0.002	0.814
2. 90° Actuator	96.4	1.01	0.006	7.29E-4	0.926
3. 180° Actuator	97.1	0.349	0.005	3.21E-4	0.976

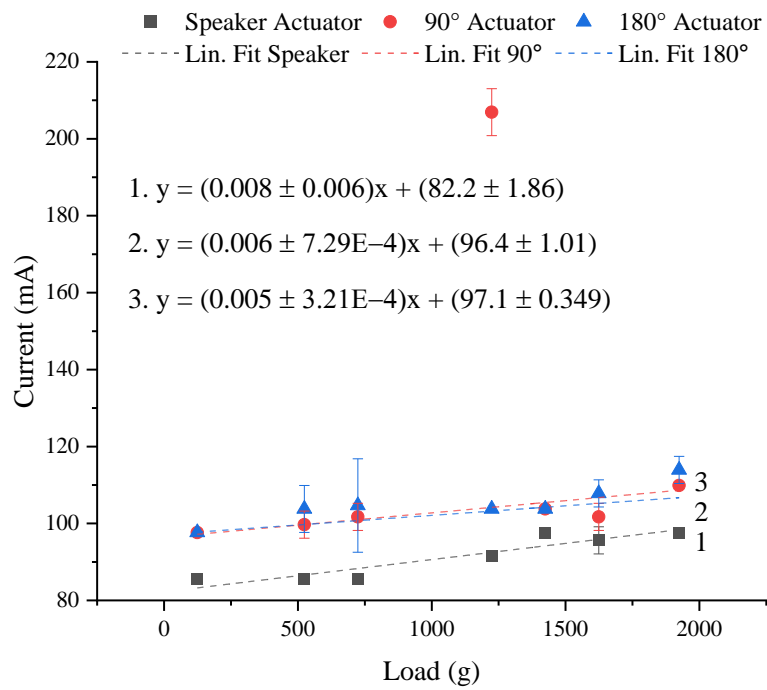


Figure 4.11. A plot of the calibration curves relating physical load applied during actuator extension and current load on the DC motor within the actuator.

The results of the load and speed calibration are shown in Table 4.3. and Figure 4.12. Table 4.3. shows the slope, intercept, and adjusted R-square value for each of the weighted linear fits. For the speaker actuator, the intercept was 0.585 ± 0.004 with a slope of $-1.08\text{E-}5 \pm 2.30\text{E-}6$. For the 90° actuator, the intercept was 0.584 ± 0.001 with a slope of $-9.96\text{E-}6 \pm 1.15\text{E-}6$. For the 180° actuator, the intercept was 0.584 ± 0.005 with a slope of $-1.17\text{E-}5 \pm 3.73\text{E-}6$. The adjusted R-square values for the speaker, 90° , and 180° actuators were 0.777, 1.00, and 0.595, respectively. The speeds of each actuator compared at the same load are not significantly different across all

Table 4.3. The intercept, slope, standard error (SE), and the adjusted R-square value for the load versus speed calibration data.

	Intercept		Slope		Adj. R-Square
	Value	SE	Value	SE	
1. Speaker Actuator	0.585	0.004	-1.08E-5	2.30E-6	0.777
2. 90° Actuator	0.584	0.001	-9.96E-6	1.15E-6	1.00
3. 180° Actuator	0.584	0.005	-1.17E-5	3.73E-6	0.595

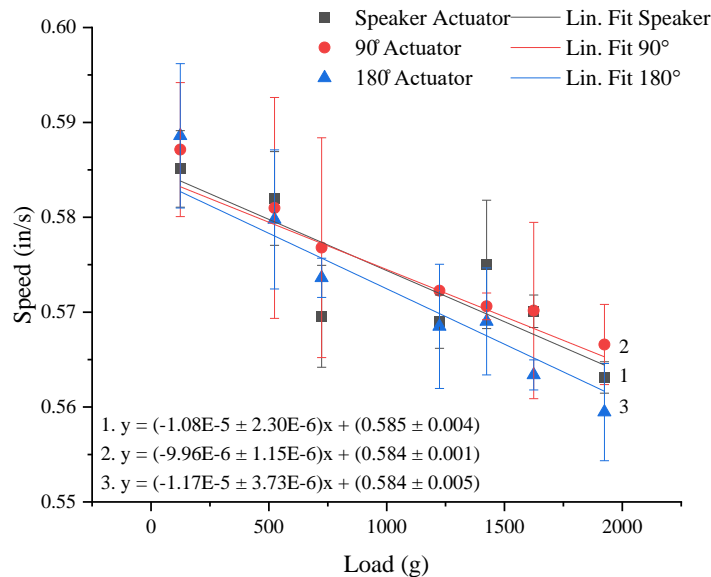


Figure 4.12. A plot of the calibration curves relating physical load applied during actuator extension and the extension speed of the linear actuator.

three actuators at the 95% confidence level. The slopes of the load versus speed calibration curves are significantly different from zero at the 95% confidence level.

4.2.4. Discussion

The results from the load versus current calibration were not consistent with the initial hypothesis that as the load applied to the actuator during extension increases the current would increase. Although this trend is seen and R-square values indicate a good fit, the range of current values is not correct. The experiment was expected to produce three total calibration curves that span the operational current range from 100 mA to 200 mA reported by the manufacturer. The measured current ranges for the experiment generally range from 80 mA to 120 mA except for a lone point that measures just over 200 mA. These points along with the outlined operational current range reported by the manufacturer are shown in Figure 4.13. An evaluation of the lone point that measured just over 200 mA revealed that the current measurement was taken just after the actuator

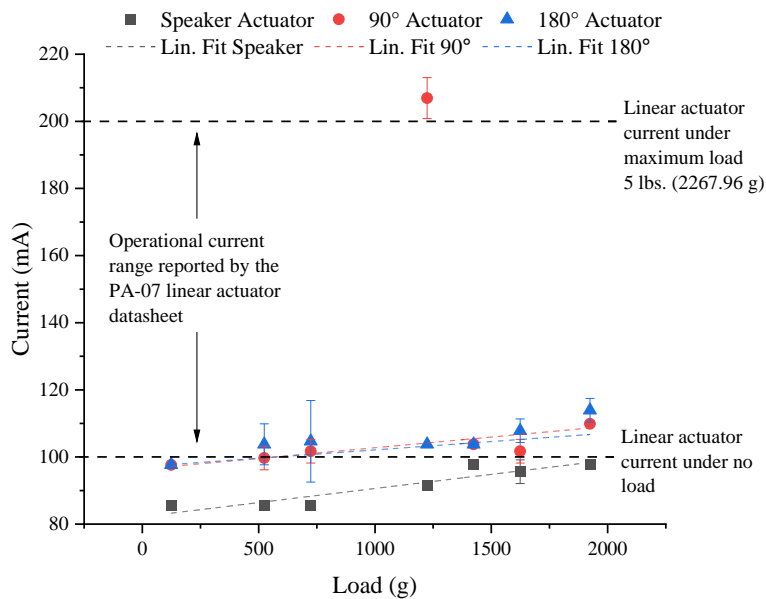


Figure 4.13. A plot of the calibration curves relating physical load applied during actuator extension and current load on the DC motor within the actuator.

had completed a full stroke length. This likely means that the motor was drawing the maximum amount of current trying to move the actuator.

The single maximum current reading led to the reconstruction of the testing protocol for the current versus load test. In the new protocol, instead of moving a known load (weight), a stopping force was applied. The stopping force was the tester physically stopping the motion of the actuator with their hand. Additionally, the power provided to the actuator was limited using a series resistor. By limiting the power seen by the actuator the coupling force and speed could be qualitatively regulated meaning that as the current decreased, the force and speed of the actuator decreased.

The results from the updated testing protocol are shown in Figure 4.14. and are qualitatively consistent with the idea that as the current decreases, the stopping force and speed of the actuator decrease. Figure 4.14. shows the current measured by the current sensors under test conditions. For the test labeled “No Load” and “Max Load” the current was not regulated by a series resistor. The tests differ because, in the “No Load” test, the actuator was not stopped by the tester while the “Max Load” test was. Limiting the current and applying a stopping force, means that the motion of the actuator will be continuous until it is stopped by a current reading. The readings from both tests closely resemble the 100-mA and 200-mA minimum and maximum current reported by the actuator manufacturer. The test labeled “R = 100 Ω ” and “R = 80 Ω ” use a 100 Ω and 80 Ω resistor that regulate the current to 120 and 150 mA, respectively. An ANOVA test was completed and showed that each of the mean values under the different test conditions was statistically different at the 95% confidence level. Qualitative observations on the speed of the actuator and the force required for the tester to stop the system indicate that low current values correspond with a slower actuator speed and less force required to stop its motion. The quantitative

results indicate that the current sensors can read the regulated current values meaning that they can be used within the actuator feedback system. The qualitative results indicate a current and applied force calibration can be made but require more testing.

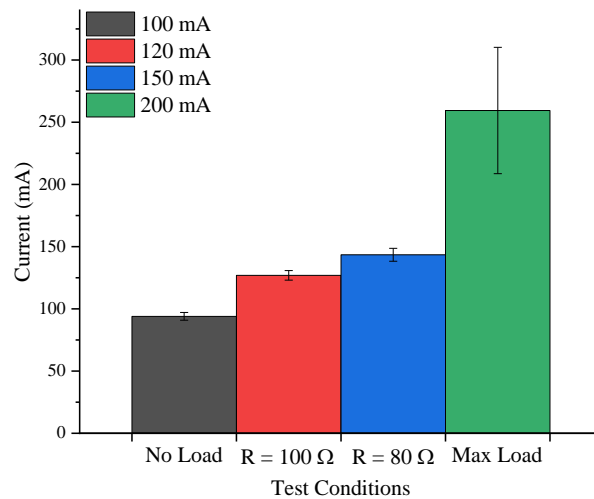


Figure 4.14. A plot of measured current regulated by a series resistor value of 0 Ω with no load, 100 Ω, 80 Ω, and 0 Ω with maximum load. At the 0 Ω conditions, no load indicates the actuator was not stopped by the tester, and max load indicates the actuator was stopped by the tester. The series of the plot (gray, red, blue, green) indicate the predicted current value.

The results from the load versus speed calibration were consistent with the initial hypothesis that as the load increases, the speed of the actuator decreases. This is evident in the negative slopes calculated for each linear trendline. The range of speeds recorded is also consistent with the manufacturer’s reported speed range of 0.59 in/s to 0.55 in/s under no load and full load, respectively. The large amount of variation associated with the speeds can be attributed to the timing mechanism used in the experiment. The time was recorded using an iPhone stopwatch with the start and stop of the timer being dependent on the tester’s ability to start and stop the stopwatch at the same time they start and end the motion of the actuator.

4.2.5. Conclusions

The results of the load versus current calibration were not consistent with the initial hypothesis that as the load applied to the actuator during extension increases the current would increase. An updated testing protocol revealed that a stopping force applied to the actuator induced the change in current that was expected. This finding has limited implications for the device because the motion of the actuators will still be stopped by a current reading although more testing is required to relate the applied force to the current. An example of an updated testing protocol might be that a pressure sensor is fixed on a static surface (i.e., a wall) and the actuator pushes against the wall under different current conditions with the applied force being recorded. The negative implication is that more work must be done to understand how the regulated current influences the speed of the actuator. The testing of the actuator while the current was not regulated was consistent with the initial hypothesis that as the load increases, the speed of the actuator decreases. This means that the speed of the actuator could be used in software-timed distance measurement.

4.3. Software Timed Distance Measurement

4.3.1. Introduction

Measuring the distance between the speaker and microphones is a critical aspect of the device as the difference in path length between the speaker and each microphone is represented in the governing equation. Since the speaker and microphones are located at the end of the three linear actuators, they can be dynamically adjusted to fit test samples and ultimately a patient's foot. This means that the position of each component must be known and relevant to one another to determine path length. This experiment builds on the Actuator Coupling Force & Speed

experiment using the speed of the actuators under load combined with a software timer to calculate the actuator's position.

4.3.2. Methods

To calculate the actuator's position, a 4" PA-07 Series Micro Linear Actuator from Progressive Automations was interfaced with LabVIEW. The actuator was controlled using a DAQ Assistant nested within a for loop and a flat sequence structure. The for loop was located within the first frame of the sequence structure which extended the actuator. An Elapsed Time function was used to control the extension time of the actuator and could be controlled by a user-defined value. After the user-defined extension time was reached, the program would move to the second frame of the sequence structure that stops the motion of the actuator. A complete diagram of the LabVIEW VI used is shown in Figure 4.15.

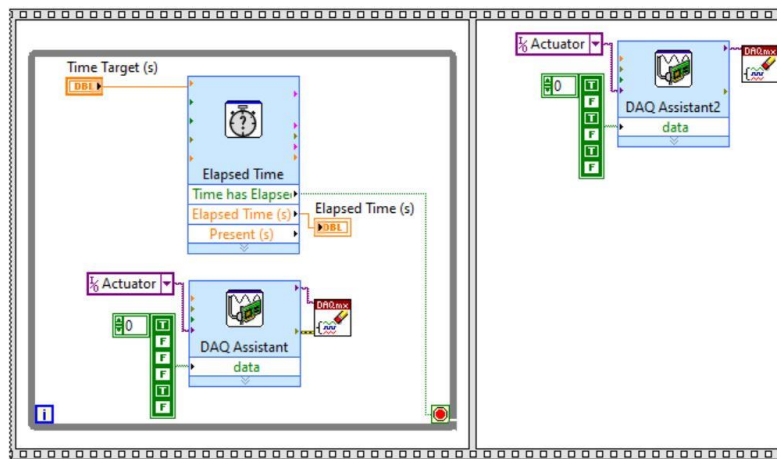


Figure 4.15. LabVIEW block diagram representation of script used during the software timed distance experiment.

A simple, three-step testing protocol was used in the experiment. The first step was to place the testing weight in front of the actuator. The second step was to set the target time in seconds and run the VI. The third step was to measure the length of the extended shaft of the actuator after

the extension was stopped with a caliper. The tests were conducted in triplicated at extension times of one through six seconds and loads of 124 g, 1224 g, and 1924 g. Figure 4.16. shows the method flow diagram of the testing protocol.

Based on the speeds measured moving known loads, the distance that the actuator traveled over a defined period could be calculated. The expected distance traveled was then compared to the measured distance traveled using a Q-Q plot. A RRMSE was used to quantify this relationship and is shown in Equation 4.1.



Figure 4.16. Method flow diagram used in the software timed distance measurement experiment where the actuator distance of the actuator pushing a known load is measured.

4.3.3. Results

The results of the software-timed distance measurement are shown in Figure 4.17 and Table 4.4. The Figure shows a Q-Q plot of the expected distance the actuator traveled versus the measured distance. The average standard error for the load at 124 g., 1224 g., and 1924 g., was 0.0054 in., 0.0039 in., and 0.0032 in., respectively. The RRMSE computed for the load at 124 g., 1224 g., and 1924 g., was 0.904%, 2.53%, and 2.70%, respectively.

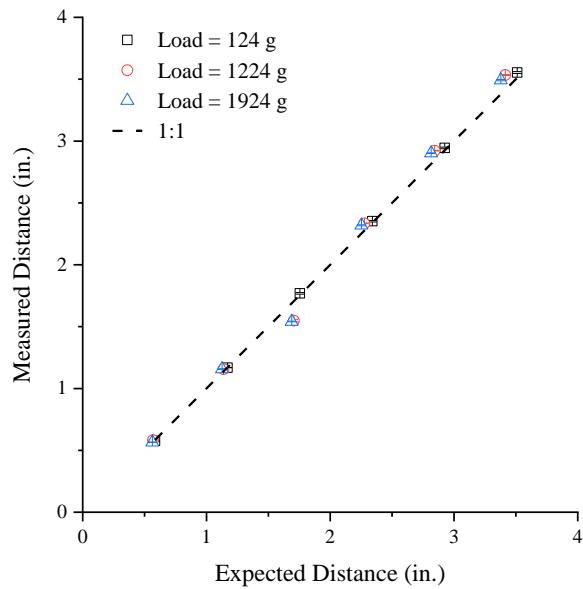


Figure 4.17. Q-Q plot of the expected distance versus the measured distance in inches (in.) for the software-timed distance measurement experiment.

Table 4.4. Shows the load applied to the actuator, the speed used to predict the expected distance, the average standard error between the expected distance and measured distance, and the RRMSE of the expected distance and measured distance.

Load (g.)	Average Speed (m/s)	Average Standard Error (in.)	RRMSE (%)
124	0.585	0.005	0.904
1224	0.568	0.003	2.53
1924	0.563	0.003	2.70

4.3.4. Discussion

The results of the software-timed distance measurement experiment show that the software timing system is effective in determining the distance the actuator traveled. The effectiveness of the timing is represented in the Q-Q plot of the expected distance based on the speed of the actuator

under load versus the measured distance of the software-controlled system. In the plot, the expected distance and measured distance follow the expected one-to-one line. This trend is shown in the low average standard error and RRMSE reported for the range of loads tested. The highest average standard error reported for the testing was 0.005 inches (0.127 mm) meaning that the software distance measurement is within five-thousandths of an inch when compared to a caliper with one thousandth of an inch resolution (0.001 inches). This means that the resolution of the distance measurement must be 0.01 inches as this is the lowest digit of agreement between the software measurement and the caliper measurement. The quality of this comparison is reflected in the low reported RRMSE values of 0.904%, 2.53%, and 2.70% where values less than 10% represent an excellent fit.⁷³ The quality of the standard error and RRMSE indicate that the software timed system is effective at determining the distance that the actuator traveled during extension with a hundredth (0.01 inches) resolution. This means that the software timed system could be applied to each actuator and the corresponding distance differences between each microphone and the speaker can be calculated relative to their fixed position in the device.

Although the software timed distance measurement shows promise in measuring the distance between the microphones and the speaker, the relays used to control the actuators should be replaced with an H-bridge controller such as the L298N Dual H-Bridge Motor Driver. The reason for this is that an H-bridge enables pulse width modulation (PWM) which provides more control over the speed and corresponding current. This means that the speed can be independently adjusted regardless of the applied load. The same type of control over the actuator speed is not currently provided by the relays as the changes in speed are only induced by changing the applied load to the actuator. The H-bridge could be controlled using the Arduino that monitors the current.

This would eliminate the need for a second MyDAQ thus reducing the cost of the prototype while providing more control.

4.3.5. Conclusion

The software timed-distance measurement system was an effective way to measure the distance of actuator extension within 0.01 inches. This means that the speed and time of actuator extension can be used to understand the distance between the microphones and the speaker. The addition of an H-bridge controller is required to independently control the speed of the actuator extension. The H-bridge can be integrated into the system by replacing the relays and eliminating the second MyDAQ. This would reduce the cost of the prototype and provide more control over the speed of the actuator.

4.4. Summary of Experimental Results

The results of the frequency and phase, actuator coupling force and speed, and software-timed distance measurement experiments indicate improvements must be made to the device. The frequency and phase experiment shows that the device can measure the frequency and phase of simulated signals. The actuator coupling force and speed experiment shows that the device is not currently able to measure the coupling force between the actuator and a test sample but the stability in the speed of the actuator under load indicates it can be used in a distance measurement. The improvements necessary to measure the coupling force between the actuator include replacing the 2-channel relays in the current system with H-bridge controllers that will use PWM to regulate the power supplied to the actuator. The regulated power can then be related to coupling force using a new testing protocol. The software timed distance measurement experiment showed that a timing system to control the motion of the actuators is effective in determining the distance up to 0.01 inches.

5. RECOMMENDATIONS FOR THE FUTURE

The goal of the project was to create a device that uses audible sound to assess bone health. For this to happen, a combination of hardware adjustments, software adjustments, and research must be completed. The primary hardware adjustment to the prototype includes replacing the 2-channel relays with H-bridge circuits for more control over the actuator motion using PWM. The software adjustment includes the writing of an Arduino script that can use PWM to control the actuators. The experimental research includes quantifying the interaction of audible sound with bone and satisfying the requirements of the FDA.

Replacing the three 2-channel relays with three L298N Dual H-Bridge Motor Drivers should improve the device as a research tool. By adding the ability to use PWM to control the actuator, the speed and force applied by the actuator can be controlled. This means that the H-bridge controller will act as both the current sensors and the relays. While the addition of the H-bridge controller will eliminate additional pieces of hardware, it will also make the device more complex from a software standpoint. This complexity can be attributed to the Arduino code that must be created to be able to apply PWM. Ultimately, the reduction in the number of hardware components and added control over the actuators outweigh the added complexity of the software.

Significant scientific questions are remaining with this research. For example, we have yet to demonstrate that audible sound can be used to effectively assess changes in BD. This work did take a critical step in the creation of a functional test bed that informs the direction of the next prototype. The next step would be to have the device measure the properties of bone phantoms. These phantoms should be composed of materials that share similar material properties to bone (i.e., density, elastic modulus, anisotropy, stiffness, and attenuation of sound). The study would focus specifically on how the propagation time between the signals at each microphone changes

concerning material properties and geometries. Special attention should be given to the computational approach to calculate density and elastic modulus within a system of equations. Frequency response curves should be generated for each material or bone phantom tested to understand individual, audible frequencies interacting with different materials. Although this approach is not solely focused on amplitude, it will likely affect the FFT approach to computing the frequency and phase of a signal. This might include a thresholding approach to selecting preferred frequencies. This work does establish a device that can be used to answer the remaining scientific questions.

Once the device can measure BD, the process of getting the device approved by the FDA can begin. This process will begin with a complete evaluation of the risks associated with the use of the device. A risk management assessment using a medical device risks management and standards like ISO 14971 or the FDA's Application of Risk Management Principles for Medical Devices. A key decision within this process will be finalizing the decision on if the device will be used in a clinical or non-clinical setting. If the device is used clinically, the risk associated with the use of the device and the interpretation of the results is mitigated because it is being used by a trained professional. If the device is used non-clinically, more effort must be made to ensure the device is easy to use. These efforts will likely include a usability study to understand how easy to use the device is. Since the device is electrical, testing the safety and performance of the components with a standard such as ANSI-60601 will likely be required. The risk management, usability, and electrical components studies will need to be accompanied by a complete description of how the device works with its intended use. A 510(k) is the expected approval pathway with the predicate or substantial equivalence being QUS. Although unlikely, there is a possibility that the FDA might require a De Novo application because the audible sound is different from

ultrasound. The key to the application will be to engage early with the FDA to better determine how the device will be regulated, although the engagement should happen when most of the studies on the device have been completed.

REFERENCES

1. Kanis, J. A. Who Scientific Group on the Assessment of Osteoporosis At Primary Health. *WHO Sci. Gr. Assess. osteoporosis Prim. Heal. care Lev.* 5–7 (2008).
2. iHealthcareAnalyst Inc. Global Osteoporosis Diagnostic Testing Market \$504 Million by 2027. (2022).
3. Brown, J. P. *et al.* Mortality in older adults following a fragility fracture: real-world retrospective matched-cohort study in Ontario. *BMC Musculoskelet. Disord.* **22**, 1–11 (2021).
4. Tabensky, A., Williams, J., DeLuca, V., Briganti, E. & Seeman, E. Bone mass, areal, and volumetric bone density are equally accurate, sensitive, and specific surrogates of the breaking strength of the vertebral body: An in vitro study. *J. Bone Miner. Res.* **11**, 1981–1988 (1996).
5. Roux, C. & Briot, K. Current role for bone absorptiometry. *Jt. Bone Spine* **84**, 35–37 (2017).
6. Morgan, S. L. & Prater, G. L. Quality in dual-energy X-ray absorptiometry scans. *Bone* **104**, 13–28 (2017).
7. Anna, U. M., Maria, S. & Kerstin, B. Comparison of quantitative ultrasound of calcaneus and dual energy X-ray absorptiometry in measuring bone density and predicting fractures in patients with diabetic polyneuropathy: A prospective cohort study. *Diabetes Res. Clin. Pract.* **180**, (2021).
8. Majumdar, S. R. *et al.* Longer duration of diabetes strongly impacts fracture risk assessment: The Manitoba BMD cohort. *J. Clin. Endocrinol. Metab.* **101**, 4489–4496 (2016).
9. Schacter, G. I. & Leslie, W. D. DXA-Based Measurements in Diabetes: Can They Predict Fracture Risk? *Calcif. Tissue Int.* **100**, 150–164 (2017).
10. Sozen, T., Ozisik, L. & Calik Basaran, N. An overview and management of osteoporosis. *Eur. J. Rheumatol.* **4**, 46–56 (2017).
11. Song, S., Guo, Y., Yang, Y. & Fu, D. Advances in pathogenesis and therapeutic strategies for osteoporosis. *Pharmacol. Ther.* **237**, 108168 (2022).
12. Snodgrass, P., Zou, A., Gruntmanis, U. & Gitajn, I. L. Osteoporosis Diagnosis, Management, and Referral Practice After Fragility Fractures. *Curr. Osteoporos. Rep.* **20**, 163–169 (2022).
13. Compston, J. E., McClung, M. R. & Leslie, W. D. Osteoporosis. *Lancet* **393**, 364–376 (2019).

14. McGregor, M., Patel, S., McLachlin, S. & Mihaela Vlasea. Architectural bone parameters and the relationship to titanium lattice design for powder bed fusion additive manufacturing. *Addit. Manuf.* **47**, 102273 (2021).
15. Wang, Q. *et al.* Multi-scale surface treatments of titanium implants for rapid osseointegration: A review. *Nanomaterials* **10**, 1–27 (2020).
16. Morgan, E. F., Unnikrisnan, G. U. & Hussein, A. I. Bone Mechanical Properties in Healthy and Diseased States. *HHS Public Access* 119–143 (2019) doi:10.1146/annurev-bioeng-062117-121139.Bone.
17. Office of the Surgeon General (US). Bone health and osteoporosis: a report of the Surgeon General. *US Heal. Hum. Serv.* 437 (2004).
18. Lang, T. F. *et al.* Volumetric quantitative computed tomography of the proximal femur: Precision and relation to bone strength. *Bone* **21**, 101–108 (1997).
19. Roy, B. Biomolecular basis of the role of diabetes mellitus in osteoporosis and bone fractures. *World J. Diabetes* **4**, 101 (2013).
20. Curry, S. J. *et al.* Screening for osteoporosis to prevent fractures us preventive services task force recommendation statement. *JAMA - J. Am. Med. Assoc.* **319**, 2521–2531 (2018).
21. ISCD. Official Positions Adult ISCD 2019. *Psychol. Appl. to Work An Introd. to Ind. Organ. Psychol. Tenth Ed. Paul* 1–34 (2019).
22. TITLE 21--FOOD AND DRUGS CHAPTER I--FOOD AND DRUG ADMINISTRATION DEPARTMENT OF HEALTH AND HUMAN SERVICES SUBCHAPTER H - MEDICAL DEVICES. *United States Food and Drug Administration* <https://www.accessdata.fda.gov/scripts/cdrh/cfdocs/cfcfr/CFRSearch.cfm?fr=892.1170> (2022).
23. *Bone Densitometer Market by Type (DEXA, Peripheral), Application (Ostopenia & Osteoporosis, Cystic Fibrosis, CKD, Body Composition Measurement, Rheumatoid Arthritis), End User (Hospitals & Specialty Clinics, Diagnostic Centres) - Global Forecast to 2027. Markets and Markets* <https://www.marketsandmarkets.com/Market-Reports/bone-densitometer-market-15369222.html> (2022).
24. X-rays. *National Institute of Biomedical Imaging and Bioengineering* <https://www.nibib.nih.gov/science-education/science-topics/x-rays#:~:text=For example%2C our bones contain,on the x-ray detector.> (2022).
25. Berger, A. Bone mineral density scans. *Bmj* **325**, 484 (2002).
26. Njeh, C. F., Boivin, C. M. & Langton, C. M. The role of ultrasound in the assessment of osteoporosis: A review. *Osteoporos. Int.* **7**, 7–22 (1997).
27. Komar, C. *et al.* Advancing methods of assessing bone quality to expand screening for osteoporosis. *J. Am. Osteopath. Assoc.* **119**, 147–154 (2019).

28. Bazzocchi, A., Ponti, F., Albisinni, U., Battista, G. & Guglielmi, G. DXA: Technical aspects and application. *Eur. J. Radiol.* **85**, 1481–1492 (2016).
29. DXA Phantom. *Sun Nuclear* <https://www.cirsinc.com/products/x-ray-fluoro/dexa-phantom/> (2023).
30. Adams, J. E. Quantitative computed tomography. *Eur. J. Radiol.* **71**, 415–424 (2009).
31. GoldSeal Optima CT660. *GE Healthcare* <https://www.gehealthcare.com/products/goldseal---refurbished-systems/goldseal-computed-tomography/goldseal-optima-ct660> (2023).
32. Agten, C. A., Ramme, A. J., Kang, S., Honig, S. & Chang, G. Cost-effectiveness of virtual bone strength testing in osteoporosis screening programs for postmenopausal women in the United States. *Radiology* **285**, 506–517 (2017).
33. Donnelly, E. Methods for Assessing Bone Quality A Review. doi:10.1007/s11999-010-1702-0.
34. European Spine Phantom. *QRM* <https://www.qrm.de/en/products/european-spine-phantom/> (2022).
35. Burgio, E., Piscitelli, P. & Migliore, L. Ionizing radiation and human health: Reviewing models of exposure and mechanisms of cellular damage. an epigenetic perspective. *Int. J. Environ. Res. Public Health* **15**, 1–13 (2018).
36. Radiation protection of patients during DXA. *International Atomic Energy Agency* <https://www.iaea.org/resources/rpop/health-professionals/other-specialities-and-imaging-modalities/dxa-bone-mineral-densitometry/patients> (2023).
37. NRC Occupational Dose Limits. *United States Nuclear Regulatory Commission* <https://www.nrc.gov/images/about-nrc/radiation/dose-limits.jpg>.
38. TITLE 21--FOOD AND DRUGS CHAPTER I--FOOD AND DRUG ADMINISTRATION DEPARTMENT OF HEALTH AND HUMAN SERVICES SUBCHAPTER H - MEDICAL DEVICES. *United States Food and Drug Administration* <https://www.accessdata.fda.gov/scripts/cdrh/cfdocs/cfcfr/CFRSearch.cfm?fr=892.1180> (2022).
39. *Global Bone Sonometer Market: By Product: Stand-Alone Bone Sonometers, Portable Bone Sonometers; Regional Analysis; Historical Market and Forecast (2017-2027); Market Dynamics: SWOT Analysis, Porter's Five Forces Analysis, EMR's Key Indicators for Demand;* <https://www.expertmarketresearch.com/reports/bone-sonometer-market> (2020).
40. Mazess, R. United States Patent - Automated Determination of Bone Morphology. (1996).
41. Achilles EXPIL. *GE Healthcare* (2017).

42. Magkos, F., Manios, Y., Babaroutsi, E. & Sidossis, L. S. Contralateral differences in quantitative ultrasound of the heel: The importance of side in clinical practice. *Osteoporos. Int.* **16**, 879–886 (2005).
43. Jurca, A., Žabkar, J. & Džeroski, S. Analysis of 1.2 million foot scans from North America, Europe and Asia. *Sci. Rep.* **9**, 1–10 (2019).
44. Pejovic-Milic, A., Brito, J. A., Gyorffy, J. & Chettle, D. R. Ultrasound measurements of overlying soft tissue thickness at four skeletal sites suitable for in vivo x-ray fluorescence. *Int. J. Med. Phys. Res. Pract.* **29**, 2687–2691 (2002).
45. Wear, K. A. Mechanisms of Interaction of Ultrasound with Cancellous Bone: A Review. *IEEE Trans. Ultrason. Ferroelectr. Freq. Control* **67**, 454–482 (2020).
46. Afzal, S. *et al.* Preparation and Evaluation of Polymer-Based Ultrasound Gel and Its Application in Ultrasonography. *Gels* **8**, (2022).
47. Drake, M. T., Clarke, B. L. & Lewiecki, E. M. The Pathophysiology and Treatment of Osteoporosis. *Clin. Ther.* **37**, 1837–1850 (2015).
48. Garcia, P. J., You, P., Fridley, G., Mabey, D. & Peeling, R. Point-of-care diagnostic tests for low-resource settings. *Lancet Glob. Heal.* **3**, e257–e258 (2015).
49. Berg, R. Sound. *Britannica* <https://www.britannica.com/science/sound-physics> (2020).
50. Crocker, M. & Arenas, J. *Noise and Vibration Control Engineering*. (Wiley, 2006).
51. Wear, K. A. The effects of frequency-dependent attenuation and dispersion on sound speed measurements: applications in human trabecular bone. *IEEE Trans. Ultrason. Ferroelectr. Freq. Control* **47**, 265–273 (2000).
52. Rho, J. Y., Kuhn-Spearing, L. & Zioupos, P. Mechanical properties and the hierarchical structure of bone. *Med. Eng. Phys.* **20**, 92–102 (1998).
53. *Medical Devices Market Size, Share & COVID-19 Impact Analysis, By Type (Orthopedic Devices, Cardiovascular Devices, Diagnostic Imaging, In-vitro Diagnostics, Minimally Invasive Surgery, Wound Management, Diabetes Care, Ophthalmic Devices, Dental Devices)*. <https://www.fortunebusinessinsights.com/industry-reports/medical-devices-market-100085>.
54. *U.S. Medical Device Manufacturers Market Size, Share, & Trends Analysis Report By Type (Diagnostic Imaging, Consumables, Patient Aids, Orthopedics), And Segment Forecasts, 2021-2028*. <https://www.grandviewresearch.com/industry-analysis/us-medical-device-manufacturers-market#:~:text=The U.S. medical device manufacturers,are the key market drivers>.
55. Point of Care Diagnostics Market Will Surpass USD 73.9 Billion by 2028 at 10.1% CAGR Growth: Says Vantage Market Research. *Vantage Market Research* (2022).

56. Newitt, P. How many orthopedic surgeons are in the US? *Beckers Orthopedic Review* [https://www.beckersspine.com/orthopedic/53833-how-many-orthopedic-surgeons-are-in-the-us.html#:~:text=There are currently 22%2C965 orthopedic,to data firm Definitive Healthcare. \(2022\).](https://www.beckersspine.com/orthopedic/53833-how-many-orthopedic-surgeons-are-in-the-us.html#:~:text=There are currently 22%2C965 orthopedic,to data firm Definitive Healthcare. (2022).)
57. FAQ about Today's Podiatrists. *American Podiatric Medical Association* <https://www.apma.org/contentfull.cfm?ItemNumber=8001#:~:text=Licensed in all 50 states,Q.>
58. The Distribution of the U.S. Primary Care Workforce. *Agency for Healthcare Research and Quality* [https://www.ahrq.gov/research/findings/factsheets/primary/pcwork3/index.html#:~:text=Primary Care Workforce Facts and Stats%2C No.&text=The U.S. primary care workforce includes approximately 209%2C000 practicing primary,care professionals \(Table 1\). \(2018\).](https://www.ahrq.gov/research/findings/factsheets/primary/pcwork3/index.html#:~:text=Primary Care Workforce Facts and Stats%2C No.&text=The U.S. primary care workforce includes approximately 209%2C000 practicing primary,care professionals (Table 1). (2018).)
59. Innovation Engineering. <https://eurekaranch.com/>.
60. Sarafrazi, N., Wambogo, E. A. & Shepherd, J. A. Osteoporosis or Low Bone Mass in Older Adults: United States, 2017-2018. *NCHS Data Brief* 1–8 (2021).
61. Overview of Medical Device Classification and Reclassification. *United States Food and Drug Administration* [https://www.fda.gov/about-fda/cdrh-transparency/overview-medical-device-classification-and-reclassification \(2017\).](https://www.fda.gov/about-fda/cdrh-transparency/overview-medical-device-classification-and-reclassification (2017).)
62. Classify Your Medical Device. *United States Food and Drug Administration* [https://www.fda.gov/medical-devices/overview-device-regulation/classify-your-medical-device \(2020\).](https://www.fda.gov/medical-devices/overview-device-regulation/classify-your-medical-device (2020).)
63. Smith, E. D., Szidarovszky, F., Karnavas, W. J. & Bahill, A. T. Sensitivity Analysis, a Powerful System Validation Technique. *Open Cybern. Syst. J.* **2**, 39–56 (2008).
64. Souzanchi, M. F., Palacio-mancheno, P., Borisov, Y. A., Cardoso, L. & Cowin, S. C. Microarchitecture and Bone Quality in the Human Calcaneus : Local Variations of Fabric Anisotropy. **27**, 2562–2572 (2012).
65. Yamada, M., Ito, M., Hayashi, K. & Nakamura, T. Calcaneus as a site for assessment of bone mineral density: Evaluation in cadavers and healthy volunteers. *Am. J. Roentgenol.* **161**, 621–627 (1993).
66. Matsukawa, M. *Bone Quantitative Ultrasound. Clinical calcium* vol. 26 (2016).
67. Njeh, C. F. The Dependence of Ultrasound Velocity and Attenuation on the Material Properties of Cancellous Bone. (1995).
68. Olsen, H. F. United States Patent - Dynamic Microphone. 20–22 (1955).
69. Suzuki, T. & Suzuki, Y. United States Patent - Condenser Microphone. vol. 1 (2007).

70. Sessler, G., Hill, M. & West, J. United States Patent - Electroacoustic Transducer. *United States Patent Office* vol. 79 1648–1648 (1986).
71. Royer, D. & Perrotta, R. United States Patent - Ribbon Microphone. vol. 1 (2002).
72. Course Notes 1 : Introduction to Biomedical Instrumentation Introduction to Biomedical Instruments. 1–13.
73. Despotovic, M., Nedic, V., Despotovic, D. & Cvetanovic, S. Evaluation of empirical models for predicting monthly mean horizontal diffuse solar radiation. *Renew. Sustain. Energy Rev.* **56**, 246–260 (2016).

APPENDIX: ADDITIONAL INFORMATION ON SONOMETRIC & DENSITOMETRIC TECHNIQUES

Table A.1. Additional information on sonometric and densitometric techniques.

	This Innovation	Dual-energy X-ray Absorptivity (DXA)	Qualitative Computed Tomography (QCT)	Quantitative Ultrasound (QUS)
Device Price	Our innovation will be < \$2,000 and will not require additional infrastructure costs.	The used – new market for a DXA machine ranges from \$16,000 - \$50,000. DXA devices require additional infrastructure costs associated with housing ionizing radiation.	The used – new market for a QCT machine ranges from \$80,000 - \$300,000. QCT device require additional infrastructure costs associated with housing ionizing radiation.	The used – new market for a QUS machine ranges from \$2,000 - \$10,000. QUS devices do not require additional infrastructure cost. This is a benefit to small facilities.
Device Size	Our innovation will be $\approx 0.61 \text{ m} \times 0.30 \text{ m} \times 0.30 \text{ m}$.	The physical footprint for a DXA device is approximately $2.87 \text{ m} \times 1.31 \text{ m} \times 1.25 \text{ m}$. There are room requirements for this device that larger hospitals can accommodate. Not used in rural facilities.	The physical footprint for a QCT device is $1.938 \text{ m} \times 3.373 \text{ m} \times 2.050 \text{ m}$. There are room requirements for this device that larger hospitals can accommodate. Not used in rural facilities.	The physical footprint for a QUS device is $0.61 \text{ m} \times 0.30 \text{ m} \times 0.30 \text{ m}$. The smaller device works well for rural care facilities where space is limited. The smaller device could also work well for a non-clinical test.
Device Safety (Single Use)	Our innovation will use audible sound, which is a lower energy level than ultrasound.	A DXA scan exposes patients to 0.1 – 1.8 mrem dependent upon the type of beam scanner	A QCT scan exposes patients to 5 - 10 mrem dependent upon the type of beam scanner	The use of ultrasound does not have the same safety concerns as densitometric techniques. Ultrasound has been reported to slightly increase tissue temperature.
Device Safety (Prolonged Use)	Our innovation will use audible sound, which is a lower energy level than ultrasound.	The use of radiation can cause lethal and prolonged damage to cells. Cumulative radiation exposure can increase the risk of certain illness and disease.	The use of radiation can cause lethal and prolonged damage to cells. Cumulative radiation exposure can increase the risk of certain illness and disease.	The use of ultrasound does not have the same safety concerns as densitometric techniques. Ultrasound is known to slightly increase tissue temperature.
Assess Bone Health	Our innovation will measure volumetric bone density (i.e., g/cm^3) and elastic modulus.	A DXA scan measures the arial density (g/cm^2) of bone or bone mineral density (BMD) and calculates a statistical metric (t or z-score) based on age and region of the scan. The statistical metric is used to differentiate between normal, osteopenic, and osteoporotic bone. This uses ionizing radiation.	A QCT scan measures arial (g/cm^2) and volumetric (g/cm^3) density and calculates a statistical metric (t or z-score) based on age and region of the scan. The statistical metric is used to differentiate between normal, osteopenic, and osteoporotic bone. This uses ionizing radiation.	A QUS scan measures broadband ultrasound attenuation (BUA) and speed of sound (SOS) to compute a stiffness index (SI). The SI is used to calculate a statistical metric (t or z-score) to differentiate between normal, osteopenic, and osteoporotic bone. This uses ultrasound.

Table A.1. Additional information on sonometric and densitometric techniques (continued).

Predictor of Osteoporotic Fracture	Our innovation will measure bone density thus giving it the ability to predict osteoporotic fracture.	DXA can be used to predict osteoporotic fracture. The prediction validity is based on the clinical reference population. If the reference population does not match the patient, misinterpretation of results is common.	QCT can be used to predict osteoporotic fracture. The prediction validity is based on the clinical reference population. If the reference population does not match the patient, misinterpretation of results is common.	QUS can be used to predict osteoporotic fracture. The prediction validity is based on the clinical reference population. If the reference population does not match the patient, misinterpretation of results is common.
Ease of Use (End User Perspective)	Our innovation will measure bone density in < 5 minutes, without the need for a calibration phantom or a statistical test result.	DXA tests measure bone density in 10-20 minutes, require a calibrating phantom, and report a statistical result (t or z-score). Special training is required to administer this test.	QCT tests measure bone density in 5-10 minutes, require a calibrating phantom, and report a statistical result (t or z-score). Special training is required to administer this test.	A QUS test measures stiffness index in 5 minutes, requiring a calibration step, fluid medium changes, and report a statistical result (t or z-score). No training is required to administer this test.

BIOGRAPHY OF THE AUTHOR

Evan Bess was born in Waterville, Maine on February 29th, 2000. He graduated from Madison Area Memorial High School in the spring of 2018 before attending the University of Maine to study Biomedical Engineering. He graduated from the University of Maine in the spring of 2022 with a bachelor's degree in biomedical engineering. He began his graduate studies during his time as a fourth-year undergraduate student in the fall of 2021. Evan is a candidate for the Master of Science degree in Biomedical Engineering from the University of Maine in August 2023.